Terrestrial records of the Early Cretaceous paleoclimate changes in the Liupanshan Basin, NW China: Evidence from sedimentology and geochemistry

Yingchun Dong
Xi'an University of Science and Technology
Xiaochen Zhao (zxcnwu@126.com)
Xi'an University of Science and Technology
Qiang Pang
PetroChina Changqing Oilfield Company
Yan Ma
NO.11 Oil Plant, PetroChina Changqing Oilfield Company
Fangpeng Du
Yan'an University
Yingtao Chen
Xi'an University of Science and Technology
Delu Li
Xi'an University of Science and Technology
Zhengzheng Mao
Xi'an University of Science and Technology
Zeyi Feng
Xi'an University of Science and Technology

Research Article

Keywords: Early Cretaceous, paleoclimate, Liupanshan Basin, Terrestrial salified lake, Geochemistry, Hothouse climate

Posted Date: March 9th, 2023

DOI: https://doi.org/10.21203/rs.3.rs-2634138/v1

Abstract

The Early Cretaceous paleoclimate has significant influence on global ecosystem and abundant clues were recorded in both marine and terrestrial sediments. However, much less studies were conducted on the terrestrial strata than the marine strata, leading to the significance of the Early Cretaceous paleoclimate in terrestrial systems is currently unclear. In this study, we present the terrestrial sedimentary characteristics and geochemical data of the upper member of the Lower Cretaceous Liupanshan Group (Liwaxia, Madongshan and Naijiahe formations) in the Liupanshan Basin (North China) and revealed the evolution of paleoenvironment and paleoclimate recorded in the terrestrial lake. The results show that the total REE concentrations of samples from these formations range from 79.94 to 195.54 ppm, 76.94 to 162.37 ppm, and 30.06 to 205.78 ppm, respectively. All samples display obvious negative Eu anomaly and negligible Ce anomaly with the enrichment of LREE and depletion of HREE. These mudstones were rich in Na_2O, TFe_2O_3 and several trace elements (e.g., Ba, Sr, and Rb) and depleted in other elements (e.g., Al_2O_3, CaO, Th, Zr, and Hf,). The major element composition and other geochemical indicators (e.g., CIA) indicate that the collected mudstones have experienced weak weathering during transportation. Based on the geochemical characteristics, the source of the Liwaxia-Naijiahe Formation has a felsic provenance, derived from the predominantly acidic magmatic rocks in the Qinling-Qilian Orogenic Belt. Multiple geochemical indicators show that the Liwaxia Formation was deposited in a semiarid-arid, anoxic, and low-moderate salinity environment, while the Madongshan-Naijiahe Formation were deposited an arid, anoxic, and high salinity environment. As a typical terrestrial salified lake in North China, the salinization of the sedimentary water bodies and the formation of black shales in the Madongshan-Naijiahe Formation might be related to an oceanic anoxic event in the hothouse climate in the Early Cretaceous.

Introduction

The Cretaceous is the unique period in Earth's history and featured by several abnormal geological events including activity of mantle superplume (Larson 1991), extraordinary igneous events (Larson 1991; Jones and Jenkyns 2001), normal superchron (Helsley and Steiner 1969; Cronin et al. 2001), and eruption of Large Igneous Provinces (LIPs; Schlanger et al. 1981; Larson 1991; Tarduno et al. 1991). These geological events further result in global paleoclimate and paleoecosystem fluctuations (e.g., Hu 2005), which were documented in ocean anoxic event (OAEs; Schlanger and Jenkyns 1976; Leckie et al. 2002; Jenkyns 2003), ocean red beds (ORBs; Hu et al. 2005, 2006, 2012a, 2012b; Wang et al. 2005, 2009), and biotic turnovers and mass extinctions (Leckie et al. 2002). More importantly, the Cretaceous is also typified as long-term “greenhouse state” (Bice et al. 2006). Multi-proxy records and climate simulations show that the Cretaceous period underwent high atmospheric CO_2 concentrations and sea levels (Bice and Norris 2002; Huber et al. 2002; Wang et al. 2014; O'Brien et al. 2017), extreme warmth of tropical sea surface temperatures (SSTs; Pearson et al. 2001; Norris et al. 2002; Wilson et al. 2002), warm deep-ocean temperatures (Friedrich et al. 2012). These paleoclimate reconstructions were largely derived from marine sedimentary successions, however, the record in terrestrial strata is rarely reported and the significance of the Cretaceous paleoclimate in terrestrial contexts in unclear. Some paleoclimate events also affected terrestrial ecosystems, such as frequent OAEs (Ludvigson et al. 2010; Li et al. 2013; Kaiho et al. 2014) and strengthening the study of terrestrial records can provide important information in revealing various features of the Cretaceous greenhouse climate (Zhang et al. 2020). Therefore, more research on terrestrial sedimentary successions is necessary. Furthermore, given current global warming trends, the study of Cretaceous warming events is also of great significance for our understanding the global warming today and evaluating the its ecological influence in the future.

Lower Cretaceous continental strata were widely deposited in the sedimentary basins of the northern China (Cao 2010, 2018; Xi et al. 2019). The Cretaceous Liupanshan Basin in the northwestern China, situated in the northern mid-latitudes of the North China Block (NCB), contains continues terrestrial fluvial-lacustrine sedimentary record available for the Cretaceous paleoenvironmental reconstructions (Dai et al. 2010; Liang et al. 2022). The Liupanshan Group contains abundant flora and fauna fossils including *Lycoptera, Caddisfly, oncolite, and Pseudofrenelopsis* (Du et al. 2014; He et al. 2014; Liang et al. 2022) and yield the age of 127 ~ 100 Ma by magnetostratigraphic data (Dai et al. 2009). These data could provide high-resolution natural archives of the paleoenvironment and paleoclimate evolution of this terrestrial basin. In the past decades, the Lower Cretaceous strata in the Liupanshan Basin (Liupanshan Group) have received significant attention due to its hydrocarbon exploration potential (e.g., Zhao et al. 2013; Han et al. 2019; Ma et al. 2021; Zhang et al. 2022). Nevertheless, the detailed paleoclimate studies were rarely carried out. The gypsum-salt rocks and black shale widely distributed in the Lower Cretaceous strata in the Liupanshan Basin may record the Cretaceous greenhouse climate on the terrestrial system. Previous studies demonstrated that the certain trace elements are suited to infer paleoenvironment, provenance, tectonic setting and other geological information related to their deposition (Wang et al. 2018 and references therein). Especially, trace elements and REEs were widely used to reconstruct paleoclimate and paleoredox conditions (e.g., Tanaka et al. 2007; Zanin et al. 2010; Bai et al. 2015). In this study, we present geochemical study for the Lower Cretaceous strata in the Liupanshan Basin. Combined with previous sedimentary, petrographic, and paleontological analysis, some significant information about paleoenvironment conditions, provenance, and evolution history of this sedimentary basin are discussed. The results of this study could help us to decipher the Cretaceous greenhouse climate records in continental strata and better understand the impact of the Early Cretaceous paleoclimate fluctuations on the biological and sedimentary evolution of paleolakes.

Geological Background

The Liupanshan Basin in the Early Cretaceous is situated in a special tectonic position, which is bounded by the Ordos Block, the Alxa Block, the Hexi Corridor Belt, and the Qinling-Qilian Orogenic Belt. The basin is now featured by an arcuate tectonic belt and a series depressions and uplifts distribution along the arc-shaped faults under the regional compressions. The Liupanshan area underwent multiple tectonic events during the Phanerozoic, characterised by complex structure characteristics and multiperiod stratigraphical break (Liu et al. 2005; Li et al. 2013; Zhao et al. 2020). The early evolution of this area was controlled by the evolution of Paleo-Qilian Ocean (Zhao et al. 2016), while transformed to an intracontinental setting in the Early Mesozoic (Darby and Ritts 2002), and has close relationship with the Ordos Basin (Bai et al. 2006; Liu et al. 2006; Zhao et al. 2006). After the Late Jurassic tectonic event separated the Liupanshan area from the Ordos Basin, the Liupanshan Basin entered into its independent evolution stage (Bai et al. 2006). During the Early Cretaceous, this basin was located in the northeastern part of the Neotethys Ocean and southwestern part of NCB in paleolatitude 31°N with a subtropical climate zone (Fig. 1a) (Yin

1988; Sun et al. 2001). The tectonic deformation and stress field inversion of the Liupanshan Basin revealed that the basin was downfaulted in the Early Cretaceous and a thick fluvial-lacustrine sequences (Liupanshan Group) were deposited (Fig. 1c) (Shi et al. 2006). Since the latest Early Cretaceous, the Liupanshan Basin was inversed and experienced regional uplift under the NW-SE compression, resulting in the eventually disappear (Shi et al. 2006; Zhao et al. 2020)

The Liupanshan Basin extends northwest with an inverted triangle shape, and can be divided into two primary structural units (the central depression and the eastern slope) and 10 secondary structural units including 5 sags, 3 highs and 2 fault terraces (Huan et al. 2011; Chen 2018; Ma et al. 2021) (Fig. 1b). The Lower Cretaceous strata (Liupanshan Group) in the basin is divided into Sanqiao Formation, Heshangpu Formation, Liwaxia Formation, Madongshan Formation and Naijiahe Formation (Fig. 1c, 2).

The Liupanshan Group is in unconformity contact with the upper and lower strata, while the 5 formations within are conformable contact (Cui et al. 2013; Chen 2018). The Sanqiao Fm. is mainly composed of conglomerate, breccia and pebbly coarse sandstone, which belongs to piedmont alluvial facies deposit (Fig. 3). The Heshangpu Fm. mainly consists of sandstone and fine sandstone with siltstone and mudstone, belonging to fluvial deposit (Fig. 3). The Liwaxia Formation is a succession of shallow to semi-deep lacustrine deposits that are dominantly purple-red and gray-green sand-mudstone (Fig. 3). The Madongshan Formation and Naijiahe Formation are generally composed of mudstone, shale and limestone with gypsum, which belong to deep lacustrine-saline lacustrine deposits (Fig. 3). Macrofossils such as plants, fishes, and insects are sporadically found in the Madongshan Fm (Li et al. 2013). In general, from bottom to top, the Cretaceous sequence in the Liupanshan Basin underwent the transformation process from piedmont-river facies to lake-saline lacustrine facies.

Sampling And Analytical Methods

To determine the geochemical features of the Cretaceous Liupanshan Basin, we selected Huoshizhai section in the central basin. A total of 23 mudstone samples were collected from the Huoshizhai section in the Liupanshan Basin: seven, six, and ten samples were from the Liwaxia Fm., Madongshan Fm., and Naijiahe Fm., respectively. The samples were collected after removing the weathering surfaces by digging to about 0.2 m. To minimize the influence of weathering and other contamination, all samples were placed in sealed plastic bags and sent to the laboratory for the subsequent experiments.

Whole-rock major and trace elements of studied samples were analyzed at the State Key Laboratory of Continental Dynamics, Northwest University, China. Fresh chips of whole rock samples were powdered to ~ 200 mesh using a tungsten carbide ball mill. Major elements were analyzed using a Rikagu RIX 2100 X-ray fluorescence (XRF) and trace elements were analyzed by an Agilent 7500a inductively coupled plasma mass spectrometry (ICP-MS) using United States Geological Survey (USGS) and international rock standards (BHVO-2, AGV-2, BCR-2 and GSP-1). For the trace element analysis, sample powders were digested using an HF + HNO_3 mixture in high-pressure Teflon bombs at 190°C for 48 hours. The analytical precision and accuracy for most of the major elements and trace elements are better than 5% and 10%, respectively (Liu et al. 2007a).

Analytical Results

Major element geochemistry

Major element contents of these mudstones of Liupanshan Basin are listed in Table 1. Major element SiO_2 is obviously enriched in these mudstones, which is ranges from 7.36–57.56%, with an average value of 38.69%, less than that of the upper continental crust (UCC). The content of Al_2O_3 (between 2.14% and 19.98%, the average proportion is 11.85%) and CaO (between 0.71% and 37.55%, the average proportion is 15.73%) are also lower than those of the UCC. The average content of Na_2O (1.44%) and TFe_2O_3(4.52%) are higher than that of the UCC. The abundances of MgO, K_2O, TiO_2, MnO and P_2O_5 are all slightly lower than that of the UCC.

Table 1
Concentrations of major-element oxides in samples from the Liupanshan Basin (units in %)

Sample	SiO_2	Al_2O_3	TiO_2	Fe_2O_3	MnO	MgO	CaO	Na_2O	K_2O	P_2O_5	SO_3	LOI	Total	Al_2O_3/TiO_2	CIA	ICV
NX-20-21	57.46	16.68	0.70	5.90	0.004	2.63	3.01	0.63	5.87	0.14	0.02	7.13	100.16	23.9	66.5	1.45
NX-20-22	18.77	4.89	0.21	1.42	0.014	1.76	37.55	0.41	1.95	0.12	0.10	32.17	99.36	22.8	58.5	15.71
NX-20-23	57.12	17.27	0.71	6.29	0.000	3.46	2.47	0.62	6.12	0.17	0.06	6.14	100.42	24.5	66.6	1.49
NX-20-24	50.29	17.09	0.69	6.70	0.049	2.99	6.17	2.57	4.00	0.21	0.05	9.44	100.23	24.7	57.2	1.90
NX-20-25	57.56	16.49	0.69	5.79	0.031	2.55	3.01	0.62	5.75	0.14	0.01	6.63	99.25	24.0	66.6	1.44
NX-20-26	56.88	16.78	0.70	6.05	0.023	3.25	2.41	0.61	5.85	0.17	0.04	6.69	99.45	24.1	66.8	1.47
NX-20-27	49.60	16.39	0.67	6.42	0.076	2.90	5.97	2.53	3.90	0.20	0.04	10.47	99.16	24.4	56.7	1.92
NX-20-28	49.76	14.80	0.59	5.26	0.059	3.41	8.24	1.72	3.62	0.16	0.13	12.58	100.33	25.0	60.7	2.33
NX-20-29	19.95	5.25	0.22	2.14	0.045	8.85	28.09	0.91	1.26	0.11	0.42	32.69	99.93	24.3	54.6	14.87
NX-20-30	40.96	11.83	0.48	4.34	0.054	8.25	10.36	1.23	2.88	0.14	0.15	19.54	100.22	24.6	62.2	4.08
NX-20-31	49.79	15.22	0.59	5.40	0.038	3.50	8.40	1.76	3.65	0.16	0.14	11.47	100.12	25.6	61.0	2.31
NX-20-32	19.71	5.42	0.22	2.19	0.019	8.74	28.15	0.86	1.31	0.12	0.39	32.70	99.82	24.7	56.1	14.37
NX-20-33	40.86	12.24	0.49	4.51	0.032	8.49	10.60	1.12	2.96	0.14	0.16	18.46	100.06	24.8	64.0	4.03
NX-20-34	46.19	14.84	0.54	5.55	0.080	6.37	6.56	1.88	3.43	0.11	0.03	14.46	100.04	27.6	60.0	2.63
NX-20-35	52.06	19.98	0.76	7.92	0.019	3.90	0.71	3.38	4.29	0.19	0.09	7.19	100.49	26.2	64.4	1.37
NX-20-36	44.55	14.50	0.59	5.36	0.088	4.31	8.75	4.01	3.52	0.08	2.46	12.22	100.45	24.8	46.0	2.86
NX-20-37	42.71	13.48	0.51	4.90	0.061	7.25	9.60	2.66	2.75	0.21	0.17	16.10	100.41	26.4	53.5	3.48
NX-20-38	31.13	7.94	0.32	2.98	0.028	4.61	24.43	1.26	2.23	0.11	1.08	23.34	99.47	24.5	54.7	7.93
NX-20-39	11.37	2.78	0.12	0.95	0.006	1.07	34.28	0.54	0.65	0.03	34.55	12.78	99.12	23.4	52.9	24.27
NX-20-40	14.24	3.70	0.16	1.45	0.022	3.37	29.60	0.60	0.89	0.05	34.35	11.51	99.92	23.9	55.7	17.70
NX-20-41	26.79	7.83	0.31	3.47	0.037	6.21	23.37	1.69	1.79	0.14	1.42	26.99	100.05	25.1	51.1	8.37
NX-20-42	44.82	15.04	0.59	7.13	0.071	6.86	6.55	1.35	4.24	0.27	0.06	13.45	100.42	25.3	62.5	2.75
NX-20-43	7.36	2.14	0.06	1.83	0.154	18.44	27.15	0.15	0.44	0.04	0.09	41.69	99.55	33.4	68.9	45.81
NX-20-43	57.46	16.68	0.70	5.90	0.004	2.63	3.01	0.63	5.87	0.14	0.02	7.13	100.16	23.9	66.5	1.45

LOI - loss on ignition; CIA - chemical index of alteration; CIW - chemical index of weathering; *data is from Yang et al. (2011).

Zheng et al. (2015) proposed a ratio of K_2O/Al_2O_3 to reflect the status of minerals mainly controlled by major elements, among which the value of K_2O/Al_2O_3 in sedimentary rocks mainly dominated by clay minerals is generally less than 0.3 (Fig. 4). The K_2O/Al_2O_3 content of mudstone samples ranges from 0.20 to 0.40 in Liupanshan Basin, with an average value of 0.26 (Fig. 4). The ratio of Liwaxia Formation is over 0.3, while those of the Madongshan Formation and Naijiahe Formation are less than 0.3, indicating that the major elements in these two formations are mainly controlled by clay minerals, and the content of K-feldspar is very low.

Trace element geochemistry

Table 2 shows the contents of the trace elements of the collected samples. On average, the concentrations of Ba (average of 460.42 ppm), Sr (average of 835.04 ppm) and Rb (average of 108.38 ppm) are dominant in the trace elements, while the others are lower than 100 ppm. Compared with the UCC and the Post Archean Australian Shale (PAAS), the Sr in the mudstone samples are enriched (the mean is 835.04 ppm) (Fig. 4). The abundance of Y (avg. 20.67) and Cu (avg. 32.61) are similar to those of the UCC, but lower than those of the PAAS. The contents of Ba (between 70.59 ppm and 1575 ppm, the mean is 460.42 ppm) are also less than that of the UCC and PAAS. The Rb contents are slightly lower than that of the PAAS. The other elements (e.g., Th, Zr, Hf, Sc, V, Cr, Co, Ni,) are relatively depleted in the UCC, and are also significantly lower than the PAAS. All mudstone samples are enriched in U, while Nb, Zr and Ti are depleted (Fig. 5). It is noteworthy that Sr is depleted in the Liwaxia formation, but it is enriched in the Madongshan and Naijiahe Formations, which is related to the positive correlation between Sr abundance and paleosalinity.

Table 2

Concentrations of trace elements in samples from the Liupanshan Basin (units in μg/g)

Sample	Sc	V	Cr	Co	Ni	Cu	Zn	Rb	Sr	Y	Zr	Nb	Cs	Ba	Hf
NX-20-21	19.07	130.50	70.35	15.25	34.01	73.32	280.9	237.8	140.2	29.50	178.5	11.8	14.23	412.9	4.877
NX-20-22	9.81	49.43	23.02	5.506	18.19	18.85	70.55	59.0	892.8	13.50	50.8	3.802	3.285	283.7	1.414
NX-20-23	18.87	135.10	74.98	11.19	26.84	31.4	103.9	240.5	183.8	23.32	131.3	11.34	13.71	1575	3.773
NX-20-24	20.51	113.80	70.82	18.32	43.55	24.89	100.8	132.2	230.9	33.48	123.7	11.79	12.85	433.5	3.624
NX-20-25	12.74	123.66	89.67	13.30	39.14	70.04	246.61	254.22	145.04	26.49	175.78	15.57	12.73	395.5	4.492
NX-20-26	13.56	133.77	90.93	7.84	31.34	24.74	74.03	260.06	193.06	21.33	137.86	14.86	12.83	1518.9	3.640
NX-20-27	13.66	107.13	95.86	14.28	45.65	18.23	74.22	154.02	233.04	28.50	120.01	14.59	11.55	425.0	3.279
Av	15.46	113.34	73.66	12.24	34.10	37.35	135.86	191.12	288.41	25.16	131.14	11.96	11.60	720.64	3.59
NX-20-28	12.68	122.36	78.95	10.61	33.79	36.33	62.49	136.15	302.12	21.74	131.31	13.32	9.72	351.9	3.485
NX-20-29	4.85	46.27	29.23	4.11	11.92	12.92	21.21	47.38	437.13	10.97	52.37	5.16	3.15	135.9	1.391
NX-20-30	10.37	101.32	104.32	8.54	41.72	32.46	49.77	112.79	1011.75	18.96	129.76	11.13	7.67	408.0	3.380
NX-20-31	17.51	127.00	66.13	14.45	35.46	40.44	79.81	133.6	308.3	24.51	121.3	10.42	10.77	385.1	3.529
NX-20-32	8.04	47.08	25.75	7.949	18.77	14.82	29.24	46.0	456.5	11.99	66.1	3.939	3.64	145.3	1.848
NX-20-33	14.13	103.20	57.73	14.19	30.74	35.95	68.56	106.6	1069	20.79	104.2	8.776	8.276	434.5	3.032
Av	11.26	91.21	60.35	9.97	28.73	28.82	51.85	97.08	597.47	18.16	100.84	8.79	7.20	310.10	2.78
NX-20-34	16.00	105.20	60.86	16.23	32.97	34.34	62.34	124.8	680.7	25.93	105.3	9.417	9.503	546.3	3.195
NX-20-35	21.11	133.60	85.77	20.22	49.62	52.82	124	167.9	2723	32.41	129.7	11.95	30.2	394.9	3.928
NX-20-36	15.91	107.90	60.28	16.69	36.70	33.27	70.07	116.6	592.4	28.81	107.6	10.23	7.661	530.8	3.199
NX-20-37	13.63	95.47	56.72	14.6	28.59	22.13	69.68	113.3	513.4	23.14	104.0	8.892	10.68	435.4	3.035
NX-20-38	8.73	64.55	36.03	12.86	27.75	27.03	36.65	78.0	2041	16.47	74.7	6.118	5.298	603.1	2.181
NX-20-40	2.04	20.02	12.37	5.573	15.32	10.08	14.55	21.6	2868	5.26	25.5	1.884	1.691	365.8	0.703
NX-20-41	2.75	22.84	17.04	6.132	16.98	9.544	18.62	28.8	2160	6.64	27.9	2.399	2.214	142.8	0.856
NX-20-42	7.60	76.28	39.31	13.17	30.90	32.62	65.09	65.0	1787	15.90	58.7	5.905	5.537	216.4	1.719
NX-20-43	14.89	125.80	85.59	20.66	38.23	23.67	106.6	153.5	116.6	26.29	112.3	11.47	18.98	378.6	3.291
NX-20-44	2.22	57.01	117.8	16.64	25.22	70.17	69.64	17.3	120.1	9.37	12.9	1.226	1.829	70.59	0.388
Av	10.49	80.87	57.18	14.28	30.23	31.57	63.72	88.68	1360.22	19.02	75.86	6.95	9.36	368.47	2.25
UCC	14	107	83	17	44	25	71	112	350	22	190	12	4.6	550	5.8

Table 2 (Continued)

Sample	La	Ce	Pr	Nd	Sm	Eu	Gd	Tb	Dy	Ho	Er	Tm	Yb	
NX-20-21	37.65	73.88	8.58	32.45	6.353	1.286	6.104	0.934	5.024	1.004	3.052	0.427	2.869	
NX-20-22	18.65	33.53	3.48	13.04	2.391	0.518	2.349	0.381	2.130	0.418	1.304	0.190	1.356	
NX-20-23	29.50	57.94	6.78	25.22	4.878	0.916	4.588	0.728	3.829	0.791	2.403	0.361	2.338	
NX-20-24	40.80	80.72	9.10	34.87	6.930	1.432	6.685	1.031	5.724	1.100	3.214	0.449	3.036	
NX-20-25	36.01	72.31	8.55	29.79	5.955	1.18	5.601	0.79	4.458	0.91	2.546	0.39	2.605	
NX-20-26	29.78	59.17	7.03	25.31	4.920	1.31	4.464	0.63	3.592	0.75	2.134	0.33	2.210	
NX-20-27	39.26	80.44	9.21	32.16	6.416	1.30	6.104	0.86	4.799	0.97	2.698	0.41	2.694	
Av	33.09	65.43	7.53	27.55	5.41	1.14	5.13	0.76	4.22	0.85	2.48	0.37	2.44	
NX-20-28	32.64	65.39	7.37	26.22	5.115	1.01	4.764	0.66	3.706	0.75	2.081	0.32	2.167	
NX-20-29	16.89	32.98	3.66	12.99	2.504	0.49	2.446	0.34	1.881	0.38	1.048	0.16	1.022	
NX-20-30	26.65	54.77	6.10	21.84	4.363	0.89	4.101	0.57	3.176	0.65	1.841	0.28	1.889	
NX-20-31	34.91	68.58	7.65	28.57	5.394	1.091	4.902	0.784	4.176	0.813	2.481	0.353	2.313	
NX-20-32	17.64	34.41	3.73	13.95	2.710	0.512	2.482	0.390	2.025	0.408	1.145	0.171	1.044	
NX-20-33	27.31	55.50	6.04	22.45	4.423	0.893	4.310	0.677	3.581	0.706	2.197	0.295	1.993	
Av	26.01	51.94	5.76	21.00	4.08	0.81	3.83	0.57	3.09	0.62	1.80	0.26	1.74	
NX-20-34	33.00	64.63	7.36	27.79	5.454	1.154	5.318	0.839	4.565	0.887	2.600	0.341	2.278	
NX-20-35	43.64	84.97	9.86	36.48	7.306	1.447	6.720	1.076	5.773	1.126	3.364	0.477	3.091	
NX-20-36	38.51	79.11	8.64	31.86	6.168	1.264	5.921	0.947	4.968	0.955	2.883	0.377	2.629	
NX-20-37	31.62	63.26	6.97	25.54	5.125	0.980	4.571	0.734	3.923	0.782	2.353	0.335	2.226	
NX-20-38	21.88	43.99	4.85	18.27	3.394	0.665	3.352	0.514	2.771	0.536	1.684	0.235	1.496	
NX-20-40	6.37	12.50	1.38	5.23	1.007	0.197	1.000	0.168	0.853	0.177	0.537	0.070	0.501	
NX-20-41	8.63	17.31	1.88	7.17	1.426	0.257	1.213	0.211	1.145	0.225	0.662	0.100	0.620	
NX-20-42	21.45	43.75	4.76	17.97	3.236	0.631	3.351	0.499	2.703	0.515	1.606	0.229	1.471	
NX-20-43	39.62	80.50	8.94	33.28	6.327	1.126	5.584	0.866	4.656	0.885	2.539	0.354	2.206	
NX-20-44	12.10	22.94	2.34	8.61	1.587	0.340	1.735	0.274	1.412	0.299	0.847	0.124	0.765	
Av	25.68	51.30	5.70	21.22	4.10	0.81	3.88	0.61	3.28	0.64	1.91	0.26	1.73	
UCC	30	64	7.1	26	4.5	0.88	3.8	0.64	3.5	0.8	2.3	0.33	2.2	0.32

Note: $\delta Eu = Eu_N/(Sm_N \times Gd_N)^{1/2}$; $\delta Ce = Ce_N/(La_N \times Pr_N)^{1/2}$, N stands for chondrite normalized values, the chondrite data are from Sun and McDonough, 198

Rare earth element geochemistry

The concentrations of REE (rare earth elements) and some other parameters are presented in Table 2. The total amount of rare earth elements ($\sum$REE) ranges from 30.06 to 205.78 ppm with an average of 132.24 ppm (Fig. 4), which are lower than those of the PAAS (183.00 ppm) and North American Shale Composite (NASC, 173.21 ppm). The LREE (light rare earth elements) contents of mudstones from the Liwaxia, Madongshan and Naijiahe formations are significantly enriched relative to HREE (heavy rare earth elements), and the patterns exhibit pronounced fractionations between the LREE (ranges from 26.68 to 183.70 ppm, average of 118.55 ppm) and HREE (ranges from 3.38 to 21.69 ppm, average of 13.69 ppm). The average $\sum$HREE and $\sum$LREE contents are lower than those of the NASC and PAAS, and the LREE/HREE (between 7.89 and 9.75, average of 8.68) is also slightly lower than that of the PAAS but slightly higher than NASC (Fig. 4), indicating the slight enrichment in the LREE. The chondrite-normalized REE patterns are shown in Fig. 5. They are marked by significantly sloping LREE trends accompanied by flat HREE trends and the distribution patterns of the three groups are basically similar, with δEu ranging from 0.89 to 1.32(avg. 0.97) (Fig. 4), showing obvious negative Eu anomaly characteristics (Fig. 5).

Discussion

Provenance analyses

Paleoweathering and sedimentary recycling

The geochemical features of clastic rocks are strongly influenced by the existence and degree of chemical weathering and sedimentary recycling (Nesbitt and Young 1982; Krzeszowska 2019; Bokanda et al. 2021; Omietimi et al. 2022), thus a variety of different weathering conditions can be used to evaluate chemical weathering history of the source area (Nesbitt and Young 1982; McLennan et al. 1993; Fedo et al. 1995; Lewin et al. 2018). CIA values can be calculated by the formula $[Al_2O_3/(Al_2O_3 + CaO^* + Na_2O + K_2O)] * 100$ (molar proportion; Nesbitt and Young 1982), and the CaO* contents were calculated based on the method described by McLennan et al. (1993). Generally, intense weathering in the source area may result in the increase of CIA values (80–100) in sediments, whereas weak weathering may cause the sediments to have relatively low CIA values (50–70) (Yan et al. 2010; Fig. 6).

The CIA values for all collected mudstones (46.0-68.9, avg. 59.1) are lower than those of the PAAS (70.36), which indicate weak chemical weathering in the source areas (Table 1, Fig. 6). The A-CN-K ternary plot is widely applied to evaluate the degree of weathering in the source areas as well (molar proportion; Fedo et al. 1995). On the A–CN–K plot, all collected mudstone samples are plotted near to the plagioclase–K-feldspar join line and clustered between granodiorite and granite average compositions (Fig. 6). In addition, the linear weathering trend of these mudstones on the A–CN–K plot reflects that the source areas were stable (Fig. 6). These results indicate that the source areas of the collected mudstones were affected by a weak chemical weathering.

The index of compositional variability ($ICV= (TFe_2O_3 + K_2O + Na_2O + CaO + TiO_2) / Al_2O_3$) is widely used to evaluate sediment recycling and maturity (Cox et al. 1995; Awasthi 2017; Sahariah and Bhattacharyya 2019; Li et al. 2022). The high ICV value (> 1) indicate the first-cycle products in the tectonically active area, while the low ICV value (< 0.84) suggest intense weathering and multiple sedimentary cycles (Van de Kamp and Leake 1985; Cox et al. 1995; Chen et al. 2014). The ICV values of the Liwaxia to Naijiahe formations are between 0.85 and 13.85 (Table 1), with an average of 3.60, which is significantly greater than that of the PAAS (0.80). These values indicate that the Liwaxia to Naijiahe formations are first-cycle and compositionally immature. The Th/Sc and Zr/Sc ratios are widely used to deduce the sorting degree, compositional maturity, and heavy mineral accumulation of clastic sediments (McLennan et al. 1993; Dypvik and Harris 2001; ArmstrongAltrin et al. 2012; Wang et al. 2018). The Th/Sc and Zr/Sc ratios of all collected samples are 0.45–1.26 and 5.18–13.80, respectively. These data combined with Th/Sc–Zr/Sc diagram indicate that the LPS mudstones were little affected by sedimentary recycling (Fig. 7).

Type of source rocks

The detrital components and elemental composition of clastic rocks are controlled by its provenance (Verma and Armstrong-Altrin 2013; Xie et al. 2018; Li et al. 2022). Some trace elements (e.g., La, Zr, Th, Sc, Hf, Co) are non-migrating and provide a reliable indication of provenance (Li et al. 2022). In the provenance discrimination diagrams of these trace elements (Zr/Sc versus Th/Sc, Hf versus La/Th, and La/Sc versus Co/Th), most samples fall into the field of felsic rocks (Fig. 7). The mixed felsic/basic source was suggested in the Hf versus La/Th diagram (Fig. 7). However, the low MgO and TiO_2 contents indicate the depletion of Mg and Ti, and less mafic minerals, further excluded an abundant basic provenance (McCann 1991; Tao et al. 2016; Zhang et al. 2020; Li et al. 2022). The Al_2O_3/TiO_2 ratio is sensitive to the change of parent rocks: high ratios (19–28) indicate a felsic parent rock and low ratios (< 14) indicate mafic parent rocks (Table 1, Girty et al. 1996). As illustrated on Al_2O_3 versus TiO_2 diagram, the Al_2O_3/TiO_2 ratios (22.84–33.44) of all samples show a felsic rocks feature (Fig. 7). The TiO_2/Zr ratios increase obviously from felsic to mafic source, thus the TiO_2 versus Zr diagram can distinguish mafic, intermediate, and felsic rocks (Hayashi et al. 1997; Armstrong-Altrin et al. 2015a, b; Moradi et al. 2016; Wang et al. 2017c;Wang et al. 2018). This diagram suggests that the collected samples originated from felsic and intermediate rocks (Fig. 7). An acidic rocks source was also suggested by TiO_2 versus Ni diagram (Fig. 7). In addition, the REE's features can be used to infer the source of fine-grained sedimentary rocks: felsic source commonly displays higher LREE/HREE ratios and negative Eu anomalies, whereas mafic source demonstrates low LREE/HREE ratios and no pronounced Eu anomalies (Taylor and McLennan 1985; Roddaz et al. 2006; Kasanzu et al 2008). All samples show the characteristics of LREE enrichment and HREE depletion with obvious negative Eu anomalies, further denoting a felsic provenance (Fig. 5). Abundant intermediate-acidic rocks exposed in eastern Qilian and western Qinling areas (southwestern to the study area), which has been confirmed to be the provenance of the Sanqiao-Heshangpu formations of the Liupanshan Basin (Zhao et al. 2020). In addition, the detrital zircon ages distributions of Liwaxia and Madongshan formations are consistent with the those of the eastern Qilian and western Qinling orogens (Ning 2017). Hence, the provenance of the Liwaxia-Naijiahe Formations is generally inherited from the Sanqiao-Heshangpu period.

Based on the analysis above, it can be concluded that the provenance of the sediments of the Liwaxia-Naijiahe formations were mainly felsic acidic rocks of the eastern Qilian and western Qinling areas.

Paleoenvironment conditions

Paleoclimate condition

The Sr/Cu ratio is an important indicator to reveal the paleoclimate conditions: low Sr/Cu ratios (< 5.0) suggest a humid climate condition, and high Sr/Cu ratios (> 5.0) indicate an arid climate condition(Wang et al. 2017;Yu et al. 2021; Lerman 1989; Meng et al. 2012; Cao et al. 2015). The Sr/Cu ratios of the Liwaxia to Naijiahe formations are mostly > 5.0 (1.91–47.36, avg., 12.44; 7.62–33.84, avg. 23.58; and 1.71–284.52, avg. 76.02 respectively) (Fig. 8), indicating a semiarid-arid climate condition. The Sr/Cu values of some samples (e.g., NX-20-41 NX-20-43) of the Naijiahe formation are extremely high, with extremely high Sr and Ba contents, which probably indicate extreme arid and evaporative environments (e.g., Dai et al. 2021). The Sr/Ba ratio is not only used for reconstruction of the paleosalinity, but paleoclimate conditions as well (Wang et al. 2018). Generally, high Sr/Ba ratios (> 1.0) indicate an arid climate conditions and low Sr/Ba ratios (< 0.50) reflect a humid climate condition (Meng et al. 2012; Fu et al. 2016; Wang et al. 2018). The high Sr/Ba ratio of the Liwaxia to Naijiahe formations (0.12–3.15, avg. 0.74; 0.80–3.22, avg. 2.16, and 0.31–15.13, avg. 4.71) suggest a general arid climate conditions as well. The Rb/Sr ratio also an important indicator to reveal the paleoclimate conditions due to different geochemical properties (Chen et al. 2022). The low Rb/Sr ratios suggest an arid climate condition, and high Rb/Sr ratios indicate a humid climate condition (Zheng et al. 2015; Ma et al. 2019; Chen et al. 2022). The low Rb/Sr ratio of the Liwaxia to Naijiahe formations (0.07–1.75, avg. 1.06; 0.10–0.45, avg. 0.22, and 0.01–1.32, avg. 0.22) also suggest an arid climate condition (Fig. 8). The carbon isotope values of the *Pseudofrenelopsis* leaf collected from the Naijiahe Formation also indicate an arid or semi-arid climate during the late Albian (Du et al. 2018). In addition, the discovery of *Pseudofrenelopsis* and *Caddisfly* (Du et al. 2014; He et al. 2014), the dominant *Classopollis* (Li and Du 2006; Zhang et al. 2012), high pCO_2 estimates (Du et al. 2014), occurrence of gypsum layers and evidence of the carbon and oxygen isotopes (Li et al. 2013; Du et al. 2014) also support an arid climate condition during the late Early Cretaceous.

Paleoredox condition

Trace element ratios such as V/Cr, V/Ni, and V/Ni + V are considered to be credible redox indicators (Tonger et al. 2004; Liu et al. 2007; Li et al. 2020). Scheffler (2006) demonstrated that V/Cr ratio < 2 indicate an oxic condition, 2-4.25 reflect a dysoxic condition, and > 4.25 reveal an anoxic environment. V/Ni ratios will increase under reducing environments (> 1) and decrease under oxic conditions (< 1) (Tan et al. 2013). V/(V + Ni) ratios less than 0.45 indicate oxic conditions, and > 0.50 indicate anoxic (Liu et al. 2007). The low V/Cr ratios of the collected mudstone samples (0.48–2.15) fluctuate somewhat around the reference material, but all are in the oxic field except one (Fig. 8). The V/Ni ratios of all samples are greater than 1 with an average value of 2.87, indicating a reductive deposition (Fig. 8). The V/(V + Ni) ratios of all samples, ranging 0.57 to 0.83, plot into the anoxic (Fig. 8), and indicate moderate water stratification (Peng et al. 2012; Zheng et al. 2015).

The rare element U in water is oxidized to soluble U^{6+} under an oxidizing condition and results in the loss of U, while Th is generally present as insoluble Th^{4+} and stable under redox conditions (Morford et al. 2009). Thus, the U/Th ratio and δU value (δU = 2U/(U + Th/3)) are widely used to reconstruct the paleoredox condition. And U/Th ratios < 0.27 indicate an oxic condition, 0.27–0.50 reflect a dysoxic condition, and > 0.50 reveal an anoxic environment (Wignall and Twitchett 1966). The δU value < 1 indicate an oxic condition, and > 1 reveal an anoxic condition (Tonger et al. 2004; Wang et al. 2017). The U/Th ratios of the Liwaxia to Naijiahe formations are mostly > 0.27 (0.13–3.55, avg., 0.90; 0.77–1.99, avg. 1.50; and 0.31–2.24, avg. 0.92, respectively), indicating a dysoxic-anoxic condition (Fig. 8). This conclusion is also supported by high δU value (mostly > 1) (Fig. 8).

Paleosalinity

Paleosalinity is a significant indicator that is used to reflect the sedimentary environment of the water column in the geologic history (Cheng et al. 2021). The value of $100MgO/Al_2O_3$ can be used as an indicator for the paleosalinity (Zhang 1988; Lin et al. 2020; Stanistreet et al. 2020; Li et al. 2022). The $100MgO/Al_2O_3$ values of all samples ranging 15.45-861.64, suggest a high salinity condition. Generally, Sr is derived from a saline water column, whereas Ba is accumulated on the fine-grained clastic sediments (Wang et al. 2018, and reference therein). Sr/Ba ratio therefore is extensively used for reconstruction of the paleosalinity, and high Sr/Ba ratios (> 1.0) and low ratios (< 0.50) indicate a high-salinity or low-salinity column water, respectively (Meng et al. 2012; Fu et al. 2016; Wang et al. 2017). The relative lower Sr/Ba ratio of the Liwaxia formation (0.12–3.15, avg. 0.74) suggest a low-moderate salinity condition (Fig. 8). In contrast, the high Sr/Ba ratio of the Madongshan and Naijiahe formations (0.80–3.22, avg. 2.16, and 0.31–15.13, avg. 4.71), indicating a high-salinity condition. Upwards through the stratigraphy, the values gradually increase from the Liwaxia to Naijiahe formation, which record the highest paleosalinity values. Thus, this feature depicts the transition from freshwater to brackish water. The high salinity of the Madongshan and Naijiahe formations is also supported by appearance of gypsum crystals. In addition, the discovery of *Oncolites*, *Caddisfly* cases in the Madongshan-Naijiahe Formation further confirms high-salinity condition during this period (Zhong et al. 2010; He et al. 2014). Water salinity is closely related to paleoclimate: hot and arid climates commonly have high evaporation rates, resulting in high salinity, whereas warm and humid climates have lower evaporation rates, resulting in lower salinity (Wei et al. 2021). The discriminant parameters of paleoclimate and paleo-salinity show a similar trend (Fig. 8), indicating that the paleoclimate play a significant role in the Liupanshan basin's salinity fluctuation.

Reconstruction of the paleoclimate evolution model of the Liupanshan Basin and its implications

Based on the above geochemical analyses, combined with previous lithology, sedimentary, paleontology, and carbon burial characteristics of the Liwaxia-Naijiahe formations, the paleoclimate evolution model of the Liwaxia-Naijiahe period in the Liupanshan Basin was established (Fig. 9), so as to further discuss the impact of regional paleoclimatic changes on the paleontological and sedimentary evolution in the northern China during the Early Cretaceous.

During the Liwaxia period, the grain size of sediments became finer obviously than early stage, featured by predominant purple-red and gray-green sand-mudstone. The oil shale deposits developed, suggesting that the paleowater depth has obviously increased compared with the early stage. The variable colors of fine-grain sediments imply climatic fluctuation during this period. Previous studies also proposed different views of paleoenvironment, such as high salinity and arid (Zhong et al. 2014), or freshwater and warm environment (Jin et al. 2006; Cai 2021). Based on investigated samples, we prefer a semiarid-arid, anoxic, and low-moderate salinity condition during the Liwaxia period (Fig. 9). The different interpretation of paleoenvironment may be related to the climatic fluctuation, which is resulted by some geologically abrupt event. For instance, the mass mortality of *Lycoptera* during the Liwaxia period, was caused by a rapid redox change of the water body and toxicity of H_2S, which were interpreted as the results of eruption of LIPs and ocean anoxic events (Liang et al. 2022).

During the Madongshan-Naijiahe period, the Liupanshan basin was under an arid, anoxic, and high salinity condition (Fig. 9). The abundant *Cypridea-Mongolocypris-Liupanshannia, Lycopera-Huashia*, and *Kuntulunia- Tongxinichthys* in the Madongshan formation appeared, and dominating oil shale deposits developed, suggesting that the paleowater depth has further increased and reached the highest (Fig. 9). Semi-deep lake/deep lake facies deposits are mainly developed in the whole region (Zhao et al. 2020). In addition, the Madongshan period was the main stage of organic carbon burial in the Liupanshan basin. The grey-black oil shale deposits are developed in the stratum, and the TOC abundance reached its highest value (Cai 2021). The sporopollen (e.g., *Schizaeoisporites*, *Ephedripites*, and *Jugella*) and fossil plant taxa, and the leafy shoot morphological and epidermal structures of the present *Pseudofrenelopsis* in the Naijiahe formation indicate an arid climate as well (Du et al. 2014). The increasing of gypsum sequestration in the Naijiahe Fm. supports a gradual enhancement of salinization (Fig. 9). However, the lake level declined in the Naijiahe period, indicated by sedimentary characteristics (Qu et al. 2003), which is probably caused by extremely dry with high evaporation condition or regional uplift.

The Cretaceous is known to be a time of "hothouse climate" (Wang and Hu 2005; Zhang et al. 2020). In this study, a process of gradual drought and increasing salinity is suggested in the Liupanshan basin. Especially, the arid and anoxic climate conditions during the Madongshan-Naijiahe period probably have a close relationship with the global "hothouse climate" (Fig. 10). On a large scale, the Lower Cretaceous strata are widely distributed in northern China (Cao 2013; Xi et al. 2019), and most Early Cretaceous terrestrial basins display similar sedimentary features and basin evolution (Fig. 10). These basins were mainly filled under the rift basins system and featured by lacustrine sedimentary environments in the Aptian and deposited rich organic shale or coal, indicating a climate favorable for hydrocarbon generation. From NE to NW China, it displays a trend of intensified aridity. Although the development of coal in the NE China indicates a humid climate, the climatic fluctuation also led to the weakening or stopping of coal accumulation (Wang 2018). The enrichment of organic matter in the lake water, featured by the development of black shales, is considered caused by hot and dry continental paleoclimate and lake water salinity under the hothouse climate during the OAE 1 period (Zhang et al. 2021). The geochemical and organic carbon isotope analysis of the lacustrine sedimentary strata in the norther China basins, e.g., Liupanshan, Jiuquan, Liaoning, Jiaolai basins, revealed a good compatibility with the marine sedimentary strata during OAE 1 (Fig. 10) (Yang et al. 2007; Dai et al. 2012; Li et al. 2013; Suarez et al. 2013; Zhang et al. 2016; Zhang et al. 2021b). These evidences further support the hypothesis that OAE 1 has extensive responses in terrestrial basins in northern China. In addition, the gypsum deposits from Naijiahe formation (K_1n) of Liupanshan Basin, Zhonggou Formation (K_1z) of Jiuquan Basin, and Lianmuqin formation (K_1l) of the Junggar and Tuha basins (Cao 2010) are reliable evidence for this regional strong evaporation climate event. A semiarid climate interrupted by arid evaporation alternations was interpreted for the salinization in some lakes in NW China during the Early Cretaceous (Li et al. 2013; Zhang et al. 2021). The high contents of *Classopollis* were also observed in Lanzhou-Hekou, Yin'e, and Liupanshan basins (Zhang 2011), indicating that a hot, dry, and high-evaporation climate dominated the NW China during the middle-late Early Cretaceous. Therefore, the hothouse climate played a significant role in the development of terrestrial sediments (especially lacustrine hydrocarbon source rocks) during the late Early Cretaceous in northern China. This strengthens understanding of the paleoclimatic patterns of terrestrial lacustrine system in northern China under the background of a greenhouse climate. Also noteworthy is that the hothouse climate pattern was not stable and it was frequently interrupted by short-term cooling events, which has been confirmed by a large number of studies, such as, carbon-oxygen isotope values (Li et al. 2013; Zhang et al. 2021).

Conclusion

(1) Geochemical indicators revealed a weak weathering and negligible sedimentary recycling. The provenance of the Liwaxia-Naijiahe formations were mainly felsic acidic rocks of the eastern Qilian and western Qinling areas.

(2) A series of paleoclimate proxies (such as Th/U, Rb/Sr, etc.) reveal that Liwaxia-Naijiahe formations were deposited in a semiarid- arid and anoxic paleoclimate, and the degree of aridity and paleosalinity increases from the Liwaxia to the Naijiahe period.

(3) The extensive paleoclimatic and paleosalinity changes, and organic matter enrichment recorded in northern China were caused by the regional semiarid-arid paleoclimate in the late Early Cretaceous, which was related to ocean anoxic event 1 (OAE 1) under the global hothouse climate.

Declarations

Acknowledgements

This work is granted by the National Natural Science Foundation of China [No. 41802119], Fundamental Research Funds for the Central Universities, CHD [grant number 300102262508], China Postdoctoral Science Foundation [No. 2019M663779], Undergraduate Innovation and Entrepreneurship Training Program of Xi'an University of Science and Technology [No. S202210704088].

Conflict of interest

The authors declare no Conflicts of interest/Competing interests.

References

1. Armstrong-Altrin JS, Lee YI, Kasper-Zubillaga JJ, Carranza-Edwards A, Garcia D, Eby N, Balaram, Cruz-Ortiz NL (2012) Geochemistry of beach sands along the Western Gulf of Mexico, Mexico: implication for provenance. Chem. der-Erde 72:345-362.
2. Armstrong-Altrin JS, Machain-Castillo ML, Rosales-Hoz L, Carranza-Edwards A, Sanchez-Cabeza JA, Ruiz-Fernandez AC (2015a) Provenance and depositional history of continental slope sediments in the Southwestern Gulf of Mexico unraveled by geochemical analysis. Cont. Shelf. Res. 95:15-26.
3. Armstrong-Altrin JS, Nagarajan R, Balaram V, Natalhy-Pineda O (2015b) Petrography and geochemistry of sands from the Chachalacas and Veracruz beach areas, western Gulf of Mexico, Mexico: constraints on provenance and tectonic setting. J. S. Am. Earth Sci. 64: 199-216.
4. Awasthi N (2017) Provenance and paleo–weathering of Tertiary accretionary prism–forearc sedimentary deposits of the Andaman Archipelago, India. J. Asian Earth Sci. 150:45-62.
5. Bai Y, Wang X, Liu H, Li T (2006) Determination of the border line of the western Ordos Basin and its geodynamics background. Acta Geologica Sinica 80:792-810 **(in Chinese with English abstract)**
6. Bai Y, Liu Z, Sun P, Liu R, Hu X, Zhao H, Xu Y (2015) Rare earth and major element geochemistry of Eocene fine-grained sediments in oil shale- and coalbearing layers of the Meihe Basin Northeast China. J. Asian Earth Sci. 97:89-101.
7. Bice KL, Birgel D, Meyers PA, Dahl KA, Hinrichs KU, Norris RD (2006) A multiple proxy and model study of Cretaceous upper ocean temperatures and atmospheric CO2 concentrations. Paleoceanography 21:1-17.
8. Bice KL, Norris RD (2002) Possible atmospheric CO2 extremes of the Middle Cretaceous (late Albian–Turonian). Paleoceanography 17:22-1–22-17.
9. Bokanda EE, Fralick P, Ekomane E, Bisse, SB, Tata CN, Ashukem EN, Belinga BC (2021) Geochemical constraints on the provenance, paleoweathering and maturity of the Mamfe black shales, West Africa. J. Afr. Earth Sci. 175:104078.
10. Cai L (2021) Study on geochemistry and hydrocarbon generation evolution characteristics of Lower Cretaceous source rocks in southern Liupanshan Basin. Chinese Journal of Geology 56:1214-1226.
11. Cao H, Guo W, Shan X, Ma L, Sun P (2015) Paleolimnological environments and organic accumulation of the Nenjiang Formation in the Southeastern Songliao Basin, China. Oil Shale 32:5-24.
12. Cao K (2010) Cretaceous continental sedimentology and paleography in China. China University of Geosciences **(in Chinese with English abstract)**
13. Cao K (2018) Cretaceous terrestrial deposits in China. China Geology 3:402-414.
14. Chen H, Tang D, Chen S, Tang S (2022) Geochemical characteristics of mudstones from the lower cretaceous strata of the Jixi Basin, NE China: Implications for organic matter enrichment. International Journal of Coal Geology 249: 103904.
15. Chen J (2018) Study of sedimentary organic facies of Early Cretaceous source rocks in Liupanshan Basin. Geochemica 47: 325-334 **(in Chinese with English abstract)**
16. Chen M, Sun M, Cai K, Buslov M, Zhao G, Rubanova E (2014) Geochemical study of the Cambrian-Ordovician meta-sedimentary rocks from the northern altai-Mongolian terrane, northwestern Central Asian Orogenic Belt: implications on the provenance and tectonic setting. J. Asian Earth Sci. 96:69-83.
17. Cheng J, An Z, Liu L, Ji J, Yang J, Cheng Y (2001) Changes in the chemical composition of wind and dust on the Loess Plateau since the last 2.5 Ma and chemical weathering in inland Asia. Science in China 31(2):136-145 **(in Chinese)**
18. Cheng P, Xu Z, Kong J, Cheng R (2020) Paleoclimatic Evolution During Middle Jurassic in Southwestern Fujian and its Responses to the Tectonic Regime Transition in South China. Geotectonica et Metallogenia 44(05):1012-1024 **(in Chinese with English abstract)**
19. Cheng Y, Liu W, Wu W, Zhang Y, Tang G, Liu C, Nie Q, Wen Y, Lu P, Zhang C (2021) Geochemical characteristics of the lower Cambrian Qiongzhusi Formation in Huize area, east Yunnan: implications for paleo-ocean environment and the origin of black rock series. Arab. J. Geosci. 14:1-16.
20. Cox R, Lowe DR, Cullers RL (1995) The influence of sediment recycling and basement composition on evolution of mudrock chemistry in the southwestern United States. Geochem. Cosmochim. Acta 59:2919-2940.
21. Cronin M, Tauxe L, Constable C, Selkin P, Pick T (2001) Noise in the quite zone. Earth planet Sci lett 190: 13-30.
22. Cui H, Wang J, Yin K, Zhao H (2013) Characteristics of sedimentary evolution of Early Cretaceous in Liupanshan Basin. Journal of Xi'an University of Science and Technology 33:411-416 **(in Chinese with English abstract)**
23. Dai S, Huang Y, Zhao J, Zhu Q, Liu J, Kong L, Zhang M, Hu H (2010). The climate change during 128.11-119.05 Ma recorded by the susceptibility of the sediments of Liupanshan Group. Earth Science Frontiers 17(3):242-249 **(in Chinese with English abstract)**
24. Dai S, Liu X, Zhao J, Zhang M, Liu J, Kong L, Zhu Q, Huang Y (2012) The OAEs record in the terrestrial sediments: The geochemistry of black shales in the Liupanshan Group and its paleoclimatic implications. Earth Science Frontiers 19(4):255-259.
25. Dai S, Zhu Q, Hu H, Tang Y, Huang Y, Liu J, Long L, Fang X (2009). Magnetostratigraphy of the Liupanshan Group, Central China. Journal Of Stratigraphy 33:188-192 **(in Chinese with English abstract)**
26. Darby BJ, Ritts BD (2002) Mesozoic contractional deformation in the middle of the Asian tectonic collage: The intraplate Western Ordos fold thrust belt, China. Earth Planetary Science Letters 205:13-24.
27. Du B, Lei X, Zhang M, Wang S, Li A, Du Z (2018) Late Early Cretaceous climate and pCO_2 estimates in the Liupanshan Basin, Northwest China. Palaeogeography, Palaeoclimatology, Palaeoecology 503:26-39.
28. Du B, Zhang M, Dai S, Sun B (2014) Discovery of Pseudofrenelopsis from the Lower Cretaceous of Liupanshan Basin and its paleoclimatic significance. Cretaceous Research 48:193-204.
29. Du B, Zhang M, Dai S, Sun B (2014) Discovery of Pseudofrenelopsis from the Lower Cretaceous of Liupanshan Basin and its paleoclimatic significance. Cretaceous Research 48:193-204.

30. Dypvik H, Harris NB (2001) Geochemical facies analysis of fine-grained siliciclastics using Th/U, Zr/Rb and (Zr + Rb)/Sr ratios. Chem. Geol. 181:131-146.
31. Fedo CM, Wayne Nesbitt H, Young GM (1995) Unraveling the effects of potassium metasomatism in sedimentary rocks and paleosols, with implications for paleoweathering conditions and provenance. Geology 23:921-924.
32. Friedrich O, Norris RD, Erbacher J (2012) Evolution of middle to Late Cretaceous oceans-A 55 my record of Earth's temperature and carbon cycle. Geology 40:107-110.
33. Fu X, Wang J, Chen W, Feng X, Wang D, Song C, Zeng S (2016) Elemental geochemistry of the early Jurassic black shales in the Qiangtang Basin, eastern Tethys: constraints for palaeoenvironment conditions. Geol. J. 51:443-454.
34. Girty G, Ridge D, Knaack C, Johnson D, Al-Riyami R (1996) Provenance and depositional setting of Paleozoic chert and argillite, Sierra Nevada, California. J. Sediment. Res. 66:107-118.
35. Han W, Ai N, Li Y, Zhang Y, Guo W (2019) Occurrence and controls of shale absorbed gas in Liupanshan Basin. Petroleum Geology & Experiment, 41:127-133 **(in Chinese with English abstract)**
36. Hayashi KI, Fujisawa H, Holland HD, Ohmoto H (1997) Geochemistry of ca. 1.9 Ga sedimentary rocks from northeastern Labrador, Canada. Geochim. Cosmochim. Acta. 61:4115-4137.
37. He H, Lu Z, Weng P, Li H, Jia L, Liu C (2014) Fossil Caddisfly Cases from the Early Cretaceous Aliferous Strata in Liupanshan Basin, China. Earth Science 39(01):1-9 **(in Chinese with English abstract)**
38. Helsley CE Steiner MB (1969) Evidence for long intervals of normal polarity during the Cretaceous period. Earth Plant Sci Lett 5:325-332.
39. Hu X (2005) Middle Cretaceous abnormal geological events and global change. Earth Science Frontiers 12(2):222-230.
40. Hu X, Jansa L, Sarti M (2006) Mid-Cretaceous oceanic red beds in the Umbria–Marche Basin, central Italy: constraints on paleoceanography and paleoclimate. Palaeogeogr. Palaeoclimatol. Palaeoecol 233:163-186.
41. Hu X, Jansa L, Wang C, Sarti M, Bak K, Wagreich M, Soták J (2005) Upper Cretaceous oceanic red beds (CORBs) in the Tethys: occurrences, lithofacies, age, and environments. Cretac. Res 26:3-20.
42. Hu X, Scott RW, Cai Y, Wang C, Meline-Dobrinescu MC (2012b) Cretaceous oceanic Red beds (CORBs): different time scales and models of origin. Earth Sci. Rev. 115:217-248.
43. Hu X, Wagreich M, Yilmaz IO (2012a) Marine rapid environmental/climatic change in the Cretaceous greenhouse world. Cretac. Res.38:40-51.
44. Huan Y, Cui H, Shang Y, Zhao H (2011) Structural patterns and hydrocarbon distribution in Liupanshan Basin. Marine Geology Frontiers 27(5):31-46 **(in Chinese with English abstract)**
45. Huber BT, Norris RD, MacLeod KG (2002) Deep-sea paleotemperature record of extreme warmth during the Cretaceous. Geology 30:123-126.
46. Jenkyns (2003) Evidence for rapid climate change in the Mesozoic-Palaeogene greenhouse world. Philosophical Transactions of the Royal Society A-Mathematical Physical and Engineering Sciences 361(1810):1885-1916.
47. Jin X, Cao W (2006) Study on Cretaceous stratum system in Liupanshan region in Ningxia and its environment changes. Ningxia Engineering Technology 5:1-3 **(in Chinese with English abstract)**
48. Jones CE, Jenkyns HC (2001) Seawater strontiumisotopes, oceanic anoxic envents , and seafloor hydrothermal activity in the Jurassic and Cretaceous. Am J Sci 301:112-149.
49. Kaiho K, Katabuchi M, Oba M, Lamolda M (2014) Repeated anoxia-extinction episodes progressing from slope to shelf during the latest cenomanian. Gondwana Res. 25:1357-1368.
50. Kasanzu C, Maboko MAH, Manya S (2008) Geochemistry of finegrained clastic sedimentary rocks of the Neoproterozoic Ikorongo Group, NE Tanzania: Implications for provenance and source rock weathering. Precambrian Research 164(3-4):201-213.
51. Krzeszowska E (2019) Geochemistry of the Lublin Formation from the Lublin Coal Basin: Implications for weathering intensity, palaeoclimate and provenance. Int. J. Coal Geol. 216:103306.
52. Larson RL (1991) Latest pluse of Earth: Evidence for a mid-Cretaceous super plume. Geology 963-966.
53. Leckie RM, Bralower TJ, Cashman R (2002) Oceanic anoxic envents and plankton evilution : Biotic response to tectonic forcing during the mid-Cretaceous. Paleoceanography 17(3):10.1029/2001 PA 000623.
54. Lerman A (1989) Lakes Chemistry and Geology Physics. Geological Press, Texas.
55. Lewin A, Meihold G, Hinderer M, Dawit EL, Bussert R (2017) Provenance of sandstones in Ethiopia during Late Ordovician and Carboniferous–Permian Gondwana glaciations: Petrography and geochemistry of the Enticho Sandstone and the Edaga Arbi Glacials. Sedimentary Geology 375:188-202.
56. Li J, Tian J, Zhang X, Liang Q, Peng M (2022) Geochemical characteristics and the constraints on paleoenvironment, provenance, and tectonic setting of Precambrian Xifangshan Formation in the northwestern Tarim Basin, NW China. Journal of Petroleum Science and Engineering 208:109553.
57. Li J, Fu Y, Jiang F, Li D, Wang Y, Liu Y, Zheng W, Xing Z (2020)The geochemistry and paleoenvironment significance of the Lower Cretaceous Bayingebi formation in Yin'e Basin and paleoenvironment significance of the mudstones from Lower Cretaceous Bayingebi formation in Yin'e basin. Journal of Henan Polytechnic University(Nature Science) 41(03):48-56+65 **(in Chinese with English abstract)**
58. Li J, Du B (2006) Palynofloras from the Liupanshan Group (Cretaceous) at Anguo Town of Pingliang, Gansu. Acta Palaeontologica Sinica 45(4):498-513 **(in Chinese with English abstract)**
59. Li W, Dong Y, Guo A, Liu X, Zhou D (2013) Chronology and tectonic significance of Cenozoic faults in the Liupanshan Arcuate Tectonic Belt at the northeastern margin of the Qinghai-Tibet Plateau. Journal of Asian Earth Sciences 73:103-113.

60. Li X, Xu W, Liu W, Zhou Y, Wang Y, Sun Y, Liu L (2013) Climatic and environmental indications of carbon and oxygen isotopes from the Lower Cretaceous calcrete and lacustrine carbonates in southeast and northwest China. Palaeogeogr. Palaeoclimatol. Palaeoecol. 385:171-189.
61. Liang J, Chang X, Tao W, Feng Z, Li H, Zong H, Zheng M, Tsogochir T (2022) Taphonomy of Lycoptera Fossils and Its Paleoclimate and Paleoenvironment Significance from the Cretaceous Liwaxia Formation in Liupanshan Area. Earth Science 23.
62. Lin X, Zhang Z, Liu X, Chen N, Wu T, Zhang Y, Zhao P, Ma X, Zhou Z (2020) Geochemical characteristics of Late Triassic sandstones in the western part of Bayan Har Basin, Northern Tibetan Plateau, Western China: constraints on provenance, source weathering, tectonic setting, and palaeoenvironment. Geol. J. 55:5275-5293.
63. Liu C, Zhao H, Gui X, Yue L, Zhao J, Wang J (2006) Space-Time Coordinate of the Evolution and Reformation and Mineralization Response in Ordos Basin. Acta Geologica Sinica 80:617-638 **(in Chinese with English abstract)**
64. Liu C, Zhao H, Wang F, Chen H (2005) Attributes of the Mesozoic structure on the west margin of the Ordos Basin. Acta Geologica Sinica 79:737-747 **(in Chinese with English abstract)**
65. Liu Y, Liu X, Hu Z, Diwu C, Yuan H, Gao S (2007a) Evaluation of accuracy and long-term stability ofdetermination of 37 trace elements in geological samples by ICP-MS. Acta Petrologica Sinica 23(5):1203-1210 **(in Chinese with English abstract)**
66. Liu F, Liu Z, Liu R, Meng Q, Zhang J, Shi J, Du J (2007b) Geochemistry of oil shale from Jijuntun Formation of Eocene in Fushun Basin and its depositional environment. Global Geology 26(4):441-446 **(in Chinese with English abstract)**
67. Ludvigson GA, Joeckel RM, Lez LAG, Gulbranson EL, Rasbury ET, Hunt GJ, Kirkland JI, Madsen S (2010) Correlation of Aptian-Albian carbon isotope excursions in continental strata of the Cretaceous foreland basin, eastern Utah, U.S.A. J Sediment. Res. 80:955-974.
68. Ma F, Pan J, Ma R, Wu W, Zhang Y, Ma X (2019) Paleo-sedimentary environmental study of mud-shale member of Madongshan Formation of well Gucan-1 in Liupanshan Basin, North China Plate. Geological Review 65(5):1123-1130 **(in Chinese with English abstract)**
69. Ma Y, Pan J, Fu D, Wang Y, Wang Y, Chang D, Cheng L, Fu W (2021) The organic geochemistry, pore structure and methane adsorption/storage capacity of lacustrine shales from the Cretaceous Madongshan Formation, Liupanshan Basin, China. Journal of Natural Gas Science and Engineering 96:104287.
70. McCann T (1991) Petrological and geochemical determination of provenance in the southern Welsh Basin. Geological Society London Special Publications, 57, 215-230.
71. McLennan SM, Hemming S, McDaniel DK, Hanson GN (1993) Geochemical approaches to sedimentation, provenance, and tectonics. Special Paper of the Geological Society of America 284:21-40.
72. Meng Q, Liu Z, Bruch A, Liu R, Hu F (2012) Palaeoclimatic evolution during Eocene and its influence on oil shale mineralization, Fushun basin. China. J. Asian Earth Sci. 45:95-105.
73. Moradi AV, Sari A, Akkaya P (2016) Geochemistry of the Miocene oil shale (Hançili Formation) in the Çankırı-Çorum Basin, Central Turkey: implications for Paleoclimate conditions, source–area weathering, provenance and tectonic setting. Sediment Geol. 341:289-303.
74. Morford JL, Martin WR, Carney CM (2009) Uranium diagenesis in sediments un derlying bottom waters with high oxygen content. Geochim. Cosmochim. Acta 73:2920-2937.
75. Nesbitt HW, Young GM (1982) Early Proterozoic climates and plate motions inferred from major element chemistry of lutites. Nature 299(5885):715-717.
76. Ning OJ (2017) Depositional Evolution Of Cretaceous Basin in Liupanshan Area. Northwest University **(in Chinese with English abstract)**
77. Norris RD, Bice KL, Magno EA, Wilson PA (2002) Jiggling the tropical thermostat in the Cretaceous hothouse. Geology 30:299-302.
78. O'Brien CL, Robinson SA, Pancost RD, Sinninghe Damst´e JS, Schouten S, Lunt DJ, Alsenz H, Bornemann A, Bottini C, Brassell SC, Farnsworth A, Forster A, Huber BT, Inglis GN, Jenkyns HC, Linnert C, Littler K, Markwick P, McAnena A, Mutterlose J, Naafs BDA, Püttmann W, Sluijs A, van Helmond NAGM, Vellekoop J, Wagner T, Wrobel NE (2017) Cretaceous sea-surface temperature evolution: Constraints from TEX86 and planktonic foraminiferal oxygen isotopes. Earth-Sci. Rev. 172:224-247.
79. Omietimi EJ, Lenhardt N, Yang RC, Gotz AE, Bumby AJ (2022) Sedimentary geochemistry of Late Cretaceous-Paleocene deposits at the southwestern margin of the Anambra Basin (Nigeria): Implications for paleoenvironmental reconstructions. Palaeogeography, Palaeoclimatology, Palaeoecology 600:111059.
80. Pearson PN, Ditchfield PW, Singano J, Harcourt-Brown KG, Nicholas CJ, Olsson RK, Shackleton NJ, Hall MA (2001) Warm tropical sea surface temperatures in the Late Cretaceous and Eocene epochs. Nature 413:481-487.
81. Peng X, Wang L, Jiang L (2012) Geochemical Characteristics of the Lucaogou Formation Oil Shale in the Southeastern Margin of the Junggar Basin and Its Environmental Implications. Bulletin of Mineralogy , Petrology and Geochemistry 31(2):121-127+151 **(in Chinese with English abstract)**
82. Qu H, Li W, He X, Liang W, Li R, Wang W (2003) Discussion on sequence stratigraphy and petroleum system of the Lower Cretaceous in Liupanshan Basin. Journal of Northwest University (Natural Science Edition) 33:70-74 **(in Chinese with English abstract)**
83. Roddaz M, Viers J, Brusset S, Baby P, Boucayrand C, Hérail G (2006) Controls on weathering and provenance in the Amazonian foreland basin: Insights from major and trace element geochemistry of Neogene Amazonian sediments. Chemical Geology 226(1):31-65.
84. Sahagian D, Pinous O, Olferiev A, Zakharov V (1996) Eustatic curve for the Middle Jurassic-Cretaceous based on Russian Platform and Siberian Stratigraphy: zonal resolution. AAPG Bulletin 80:1433–1458.
85. Sahariah N, Bhattacharyya P (2019) Geochemical characteristics of the Tura Formation in parts of the Upper Assam Basin: an implication on provenance, tectonic setting and source-Area Weathering. J. Appl. Geochem. 21:1-14.
86. Scheffler K, Buehmann D, Schwark L (2006) Analysis of Late Palaeozoic glacial to postglacial sedimentary successions in South Africa by geochemical proxies-Response to climate evolution and sedimentary environment. Palaeogeography, Palaeoclimatology, Palaeoecology 240:184-203.

87. Schlanger SO, Jenkns HC, Premoli-Silva I (1981) Volcanism and vertical tectonics in the Pacific Basin related to global Cretaceous transgressions. Earth and Planet Science letter 52:435-439.
88. Schlanger SO, Jenkyns HC (1976) Cretaceous oceanic anoxic events Cause and consequence. Geologie en Mijnbouw 55:179-184.
89. Scotese CR (2002) Paleomap website. http://www.scotese.com. chris@scotese.com.
90. Scotese CR (2014) Atlas of Early Cretaceous Paleogeographic Maps, PALEOMAP Atlas for ArcGIS, Volume 2, The Cretaceous, Maps 23–31. Mollweide Projection, PALEOMAP Project, Evanston, IL.
91. Shi W, Zhang Y, Ma Y, Liu G, Wu L (2006) Formation and modification history of the Liupanshan basin on the southwestern margin of the Ordos block and tectonic stress field evolution. Geology in China 33:1067-1074 **(in Chinese with English abstract)**
92. Stanistreet IG, Boyle JF, Stollhofen H, Deocampo DM, Deino A, McHenry LJ, Toth N, Schick K, Njau JK (2020) Palaeosalinity and palaeoclimatic geochemical proxies (elements Ti, Mg, Al) vary with Milankovitch cyclicity (1.3 to 2.0 Ma), OGCP cores, Palaeolake Olduvai, Tanzania. Palaeogeogr. Palaeoclimatol. Palaeoecol. 546:109656.
93. Suarez BM, Ludvigson AG, González AL, Al-Suwaidi HA, You HL (2013) Stable isotope chemostratigraphy in lacustrine strata of the Xiagou Formation, Gansu Province, NW China (p. 143-155). In: Bojar, A.V., Melinte-Dobrinescu, M.C., Smit, J. (Eds.), Isotopic Studies in Cretaceous Research Geological Society.
94. Sun Z, Yang Z, Yang T, Lin A (2001) New Early Cretaceous paleoseomagnetic results from the Haiyuan area and its tectonic implications. Chinese Journal of Geophysics, 44(5):678-686 **(in Chinese)**
95. Tan X, Tian J, Huang J, Lin X, Ma J (2013) Material responses and accumulation patterns in cyclic sediment records of continental clastic rocks: taking the Paleogene Kongdian Formation of Wangjiagang area in Jiyang Depression as an example. Oil & Gas Geology 34(03):332-341 **(in Chinese with English abstract)**
96. Tanaka K, Akagawa F, Yamamoto K, Tani Y, Kawabe I, Kawai T (2007) Rare earth element geochemistry of Lake Baikal sediment: its implication for geochemical response to climate change during the Last Glacial/Interglacial transition. Quat. Sci. Rev. 26:1362-1368.
97. Tao S, Shan Y, Tang D, Xu H, Li S, Cui Y (2016) Mineralogy, major and trace element geochemistry of Shichanggou oil shales, Jimusaer, Southern Junggar Basin, China: implications for provenance, palaeoenvironment and tectonic setting. J. Petrol. Sci. Eng. 146:432-445.
98. Tarduno JA, Sliter WV, Kroenke L, Leckie M, Mayer H, Mahoner JJ, Musgrave R, Storey M, Winterer EL (1991) Rapid formation of Ontong Java Plateau by Aptian mantle plume volcanism. Sciences, 254: 399-403.
99. Taylor SR, McLennan SR (1985) The continental crust: Its composition and evolution. Oxford: Blackwell Scientific Publications.
100. Tonger, Liu W, Xu Y, Chen J (2004) The Discussion on Anoxic Environments and Its Geochemical Identifying Indices. Acta Palaeontologica Sinica, 22(4):365-372 **(in Chinese with English abstract)**
101. Van de Kamp PC, Leake BE (1985) Petrography and geochemistry of feldspathic and mafc sediments of the northeastern Pacifc margin. Trans. R. Soc. Edinb. Earth Sci. 76:411-449.
102. Verma SP, Armstrong-Altrin JS (2013) New multi-dimensional diagrams for tectonic discrimination of siliciclastic sediments and their application to Precambrian basins. Chem. Geol. 355:117-133.
103. Wang C, Hu X (2005) Cretaceous world and oceanic red beds. Earth Sci. Front. 12:11-21 **(in Chinese with English abstract)**
104. Wang C, Hu X, Huang Y, Scott RW, Wagreich M (2009) Overview of Cretaceous Oceanic Red Beds (CORBs): a window on global oceanic and climate change. Cretaceous Oceanic Red Beds: Stratigraphy, Composition, Origins and Paleoceanographic and Paleoclimatic Significance. SEPM Spec. Publ. 91:13-33.
105. Wang C, Hu X, Sarti M, Scott RW, Li X (2005) Upper Cretaceous oceanic red beds in southern Tibet: a major change from anoxic to oxic, deep-sea environments. Cretac. Res. 26:21-32.
106. Wang F, Liu X, Deng X, Li Y, Tian J, Li S, You J (2017) Geochemical Characteristics and Environmental Implications of Trace Elements of Zhifang Formation in Ordos Basin. Acta Sedimentologica Sinica 35(6):1265-1273 **(in Chinese with English Abstract)**
107. Wang S (2018) Model of coal-accumulation in the sequence stratigraphic framework of the Early Cretaceous in northeastern China. China University of Mining & Technology, Beijing **(in Chinese with English abstract)**
108. Wang Y, Huang C, Sun B, Quan C, Wu J, Lin Z (2014) Paleo-CO_2 variation trends and the Cretaceous greenhouse climate. Earth Sci. Rev. 129:136-147.
109. Wang Z, Fu X, Feng X, Song C, Wang D, Chen W, Zeng S (2017) Geochemical features of the black shales from the Wuyu Basin, southern Tibet: implications for palaeoenvironment and palaeoclimate. Geol. J. 52:282-297.
110. Wang Z, Wang J, Fu X, Zhan W, Yu F, Feng X, Song C, Chen W, Zeng S (2017c) Organic material accumulation of Carnian mudstones in the North Qiangtang Depression, eastern Tethys: controlled by the paleoclimate, paleoenvironment, and provenance. Mar. Pet. Geol. 88:440-457.
111. Wang Z, Wang J, Fu X, Zhang W, Armstrong-Altrin JS, Yu F, Feng X, Song C, Zeng S. (2018) Geochemistry of the Upper Triassic black mudstones in the Qiangtang Basin, Tibet: Implications for paleoenvironment, provenance, and tectonic setting. Journal of Asian Earth Sciences 106:118-135.
112. Wei Y, Li X, Zhang R, Li X, Lu S, Qiu Y, Jiang T, Gao Y, Zhao T, Song Z (2021) Influence of a paleosedimentary environment on shale oil enrichment: a case study on the Shahejie Formation of Raoyang Sag, Bohai Bay Basin, China. Front. Earth Sci. 9:736054.
113. Wignall PB, Twitchett RJ (1996) Oceanic anoxia and the end Permian mass extinction. Science 272:1155-1158.
114. Wilson PA, Norris RD, Cooper MJ (2002) Testing the Cretaceous greenhouse hypothesis using glassy foraminiferal calcite from the core of the Turonian tropics on Demerara Rise. Geology 30, 607-610.
115. Xi D, Wan X, Li G, Li G (2019) Cretaceous integrative stratigraphy and timescale of China. Science China Earth Sciences 62:256-286.

116. Xie G, Shen Y, Liu S, Hao W (2018) Trace and rare earth element (REE) characteristics of mudstones from eocene pinghu formation and oligocene huagang Formation in xihu sag, east China sea basin: implications for provenance, depositional conditions and paleoclimate. Mar. Petrol. Geol. 92:20-36.
117. Yan D, Chen D, Wang Q, Wang J (2010) Large–scale climate fluctuations in the latest Ordovician on the Yangtze block, south China. Geology 38:599-602.
118. Yang W, Li S, Jiang B (2007) New evidence for Cretaceous age of the feathered dinosaurs of Liaoning: zircon U-Pb SHRIMP dating of the Yixian Formation in Sihetun, northeast China. Cretaceous Research 28:2177-182.
119. Yins H (1988) The Palaeobiogeography of China. Beijing. China University of Geosciences Press 250-267 **(in Chinese)**
120. Yu H, Xu Z, Cheng R, Wang L, Gao D, Hu X, Zhang Z (2021) Paleoclimate Evolution and Elemental Geochemical Response during Middle Jurassic-Early Cretaceous in Tectonic Regime Transition Period in the North Yellow Sea Basin. Earth Science 46(3):1100-1118 **(in Chinese with English Abstract)**
121. Zanin YN, Eder VG, Zamirailova AlG, Krasavchikov VO (2010) Models of the REE distribution in the black shale Bazhenov Formation of the West Siberian marine basin, Russia. Chem. der-Erde. 70:363-376.
122. Zhang K, Liu R, Liu Z, Li B, Liu G, Yan X, Li L (2022) Terrestrial records of Early Cretaceous paleoclimate fluctuations in the Yin'e Basin, northern China: Evidence from sedimentology and palynomorphs in lacustrine sediments. Sedimentary Geology 432:106110.
123. Zhang M (2011) The Early Cretaceous palynoflora of the Liupanshan Group and Bayingebi Formation, and its paleoclimate and paleogeographic implications, Central China. Lanzhou University **(in Chinese with English abstract)**
124. Zhang M, Dai S, Zhang Y, Miao Y, Liu J, Huang Y, Zhao J, Liu X (2012) Early Cretaceous palynological assemblage and its environmental significance in the sediments of Liupanshan Group (Sikouzi Section), Liupanshan region, central China. Arid and Geography 35(1):99-108 **(in Chinese with English abstract)**
125. Zhang S (1988) Application and research of Mg/Al ratio in the sedimenatry rocks. Bulletin of Mineral Geochemistry 7(2):112-113.
126. Zhang T, Peng H, Chen J, Pan J, Liu C, Wang J (2022) Tectono-thermal evolution history and geological significance of Guyuan Depression in Liupanshan Basin. Fault-Block Oil & Gas Field 29:337-343 **(in Chinese with English abstract)**
127. Zhang X, Li S, Wang X, Zhao X, Yin T (2021b) Expression of the early Aptian Oceanic Anoxic Event (OAE) 1a in lacustrine depositional systems of East China. Global and Planetary Change 196:103370.
128. Zhang X, Zhang G, Sha J (2016) Lacustrine sedimentary record of early Aptian carbon cycle perturbation in western Liaoning, China. Cretaceous Research 62:122-129.
129. Zhang X, Gao Z, Fan T, Xue J, Li W, Zhang H, Cao F (2020) Element geochemical characteristics, provenance attributes, and paleosedimentary environment of the Paleogene strata in the Lenghu area, northwestern Qaidam Basin. J. Petrol. Sci. Eng. 195:107750.
130. Zhang X, Li S, Wang X, Zhao X, Yin T (2021) Expression of the early Aptian Oceanic Anoxic Event (OAE) 1a in lacustrine depositional systems of East China. Global and Planetary Change 196:103370.
131. Zhang X, Li S, Yan M, Wang X, Geng G (2020) Early Cretaceous black shale in the Fajiaying Formation (Lingshan Island, East China): Terrestrial record of hothouse climate. Journal of Asian Earth Sciences 191:104200.
132. Zhang X, Li S, Yan M, Wang X, Geng G (2020) Early Cretaceous black shale in the Fajiaying Formation (Lingshan Island, East China): Terrestrial record of hothouse climate. Journal of Asian Earth Sciences 191:104200.
133. Zhao H, Cui H, Wang J, Hou X, Ji J, Zhao X (2013) Structural pattern of the southwestern margin in the Liupanshan basin and its significance of petroleum prospecting. Journal of Northeast Petroleum University, 37(4), 9-17 **(in Chinese with English abstract)**
134. Zhao W, Wang X, Guo Y, Liu H, Bai Y (2006) Restoration and tectonic re working of the Late Triassic basin in western Ordos Basin. Petroleum Exploration and Development 33:6-13 **(in Chinese with English abstract)**
135. Zhao X, Liu C, Wang J, Luo W, Du F, Ma L (2020) Provenance analyses of Lower Cretaceous strata in the Liupanshan Basin: from paleocurrents indicators, conglomerate clast compositions, and zircon U-Pb geochronology. Journal of Earth Science 31:757-771.
136. Zhao X, Liu C, Wang J, Zhao Y, Wang L, Zhang Q (2016) Detrital zircon U–Pb ages of Paleozoic sedimentary rocks from the eastern Hexi Corridor Belt (NW China): Provenance and geodynamic implications. Sedimentary Geology 339:32-45.
137. Zheng Y, Ma Z, Wang B, Yuan G, Qin J (2015) Geochemistry characteristics and sedimentary environment of oil shale from the Eocene Bahuli Formation in Liushuhe Basin Heilongjiang Province. Journal of Palaeogeography 17(5):689-698.
138. Zhong F, Zhong J, You W, Bian Q, Wang J, Wang A, Meng W, Abdurahman A (2014) Lacustrine Stromatolites from The Lower Cretaceous Liwaxia Formation In The Liupan Mountain Area. Journal of Stratigraphy 38:65-70 **(in Chinese with English abstract)**

Figures

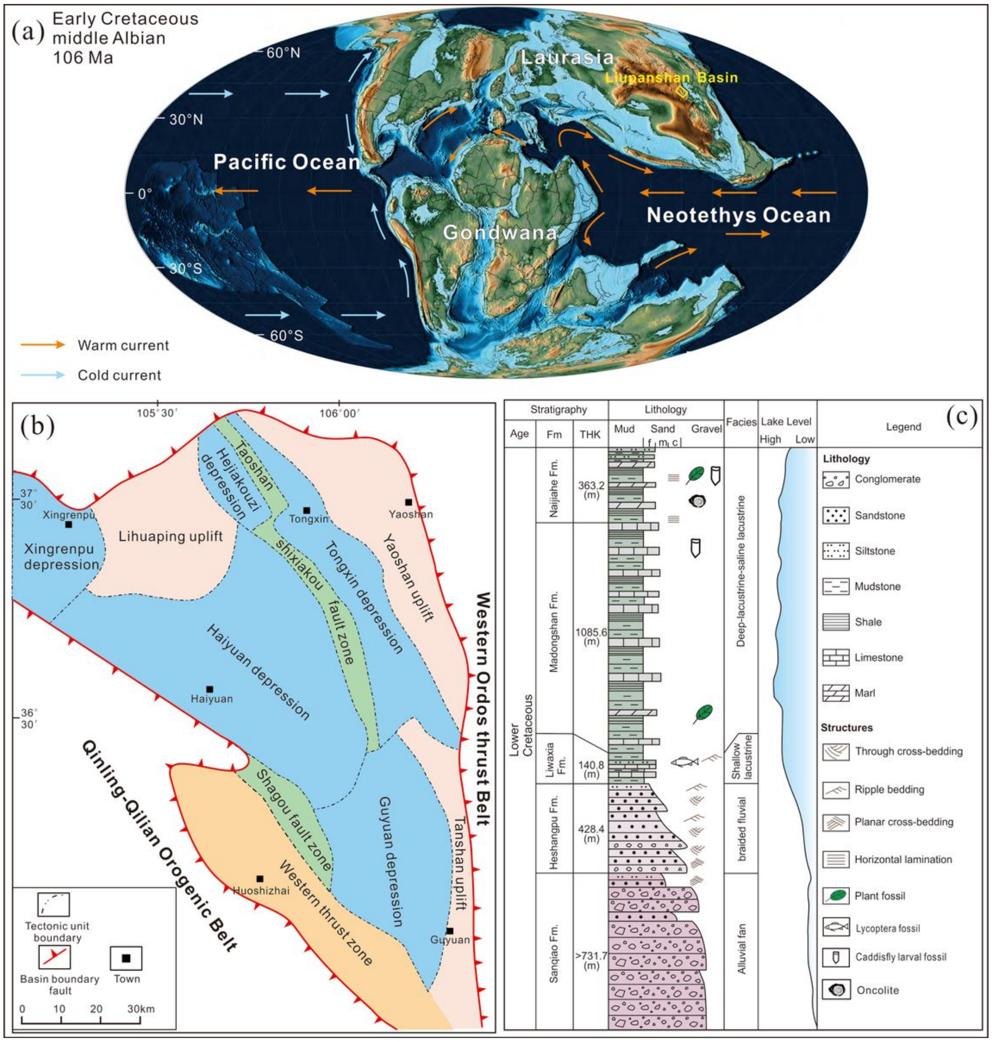

Figure 1

(a) Paleogeographic map of Albian stage (~106 Ma) of Early Cretaceous and the location of Liupanshan Basin. Map data from Scotese (2014), current data according to Scotese (2002) (b) Division of structural units in the Liupanshan Basin (modified from Cai, 2021). (c) Synthetical lithostratigraphic column of the Lower Cretaceous of the Liupanshan Basin (Zhao et al, 2020).

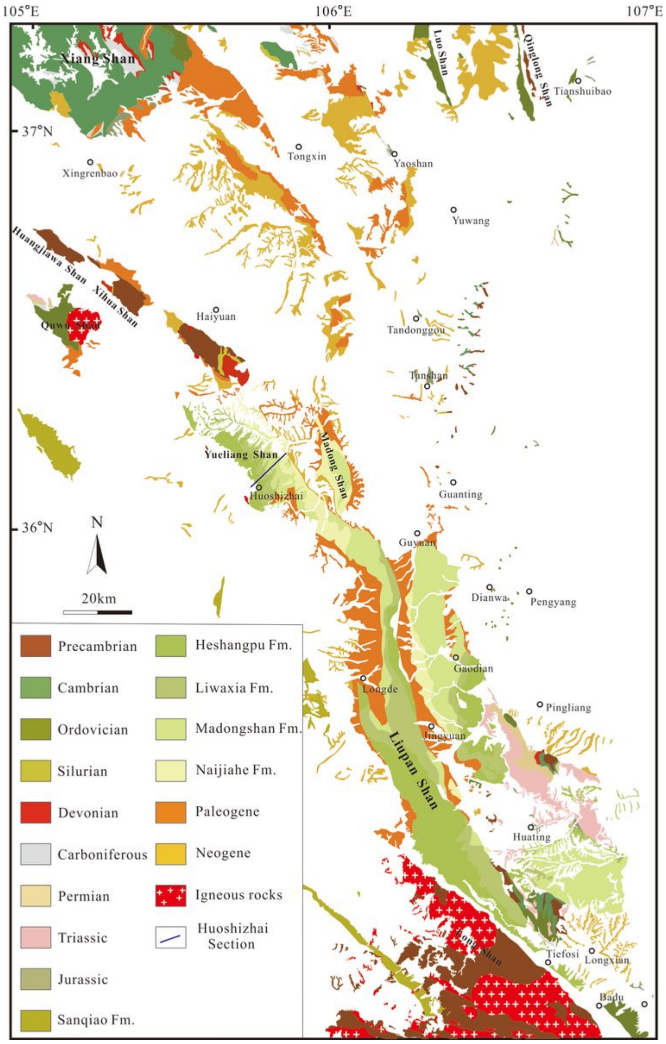

Figure 2

Geological map of the Ningnan region (modified from Zhao et al, 2020).

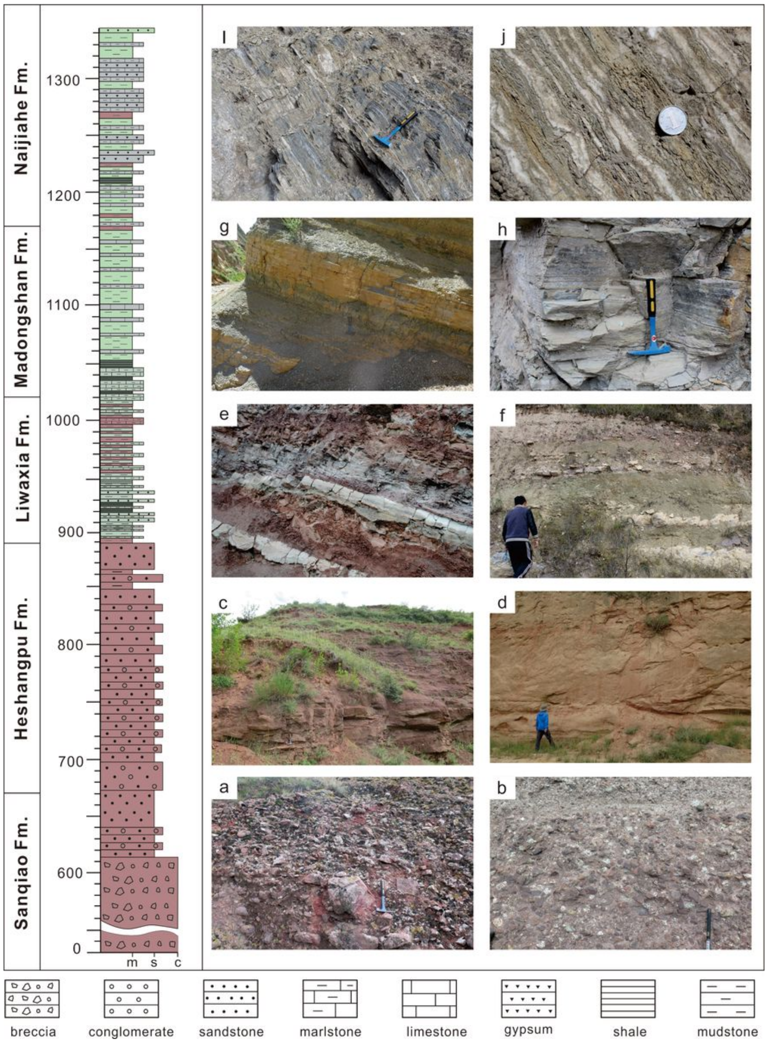

Figure 3

Lithostratigraphic column and outcrop photographs of the Huoshizhai section in the Liupanshan Basin. (a)-(b) Sanqiao Fm., (c)-(d) Heshangpu Fm., (e)-(f) Liwaxia Fm., (g)-(h) Madongshan Fm., (i)-(j) Naijiahe Fm.

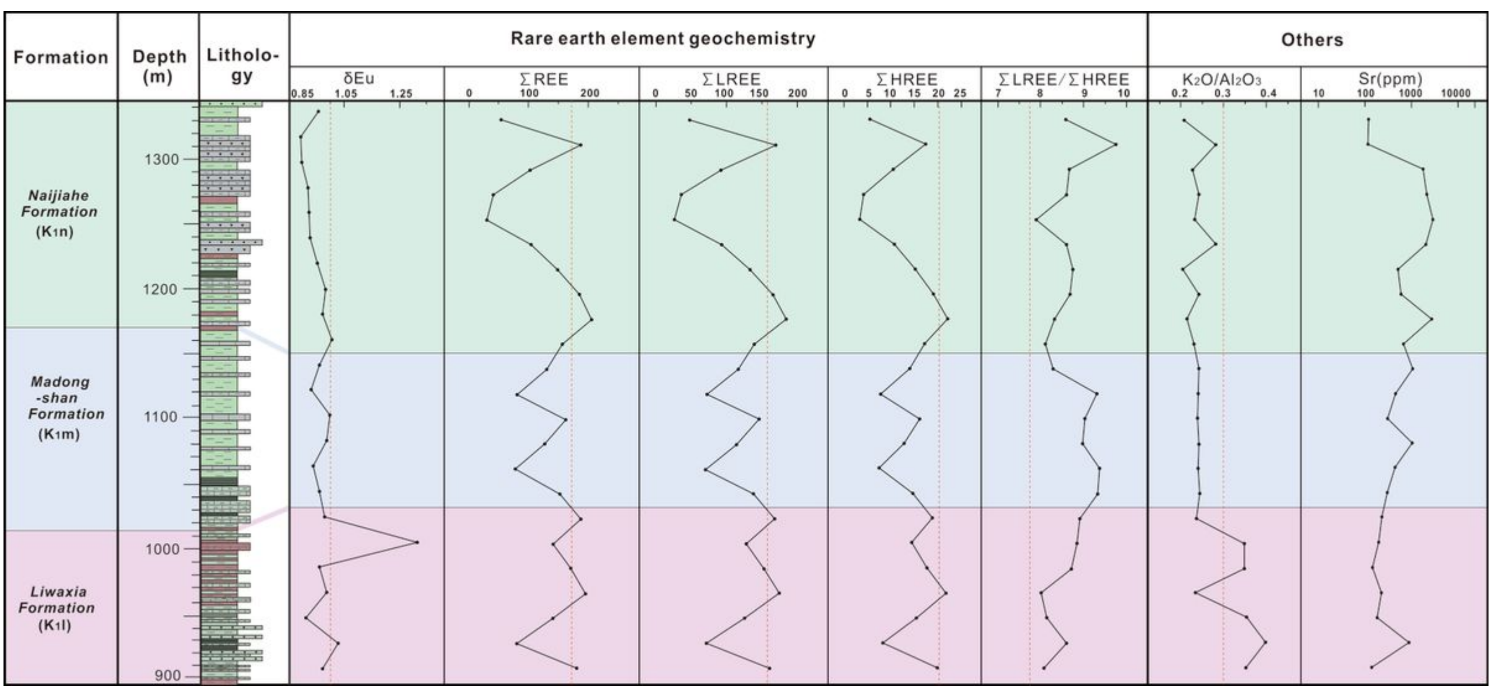

Figure 4

The geochemical profile of the Liwaxia-Naijiahe Formation in the Huoshizhai Section.

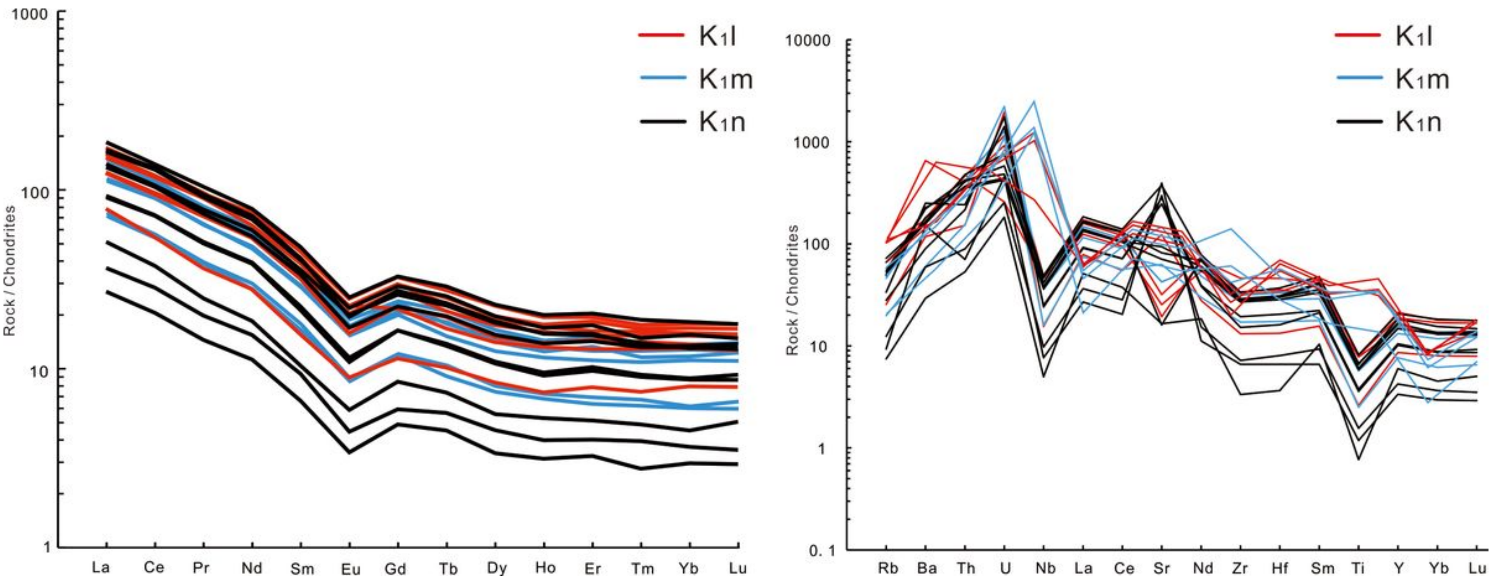

Figure 5

(a) Chondrite-normalized REE patterns of the Lower Cretaceous mudstones from the Liupanshan Basin; (b) Chondrites-normalized multi-element diagrams for trace elements in the Lower Cretaceous mudstones from the Liupanshan Basin. Chondrite values are from Taylor and McLennan (1985).

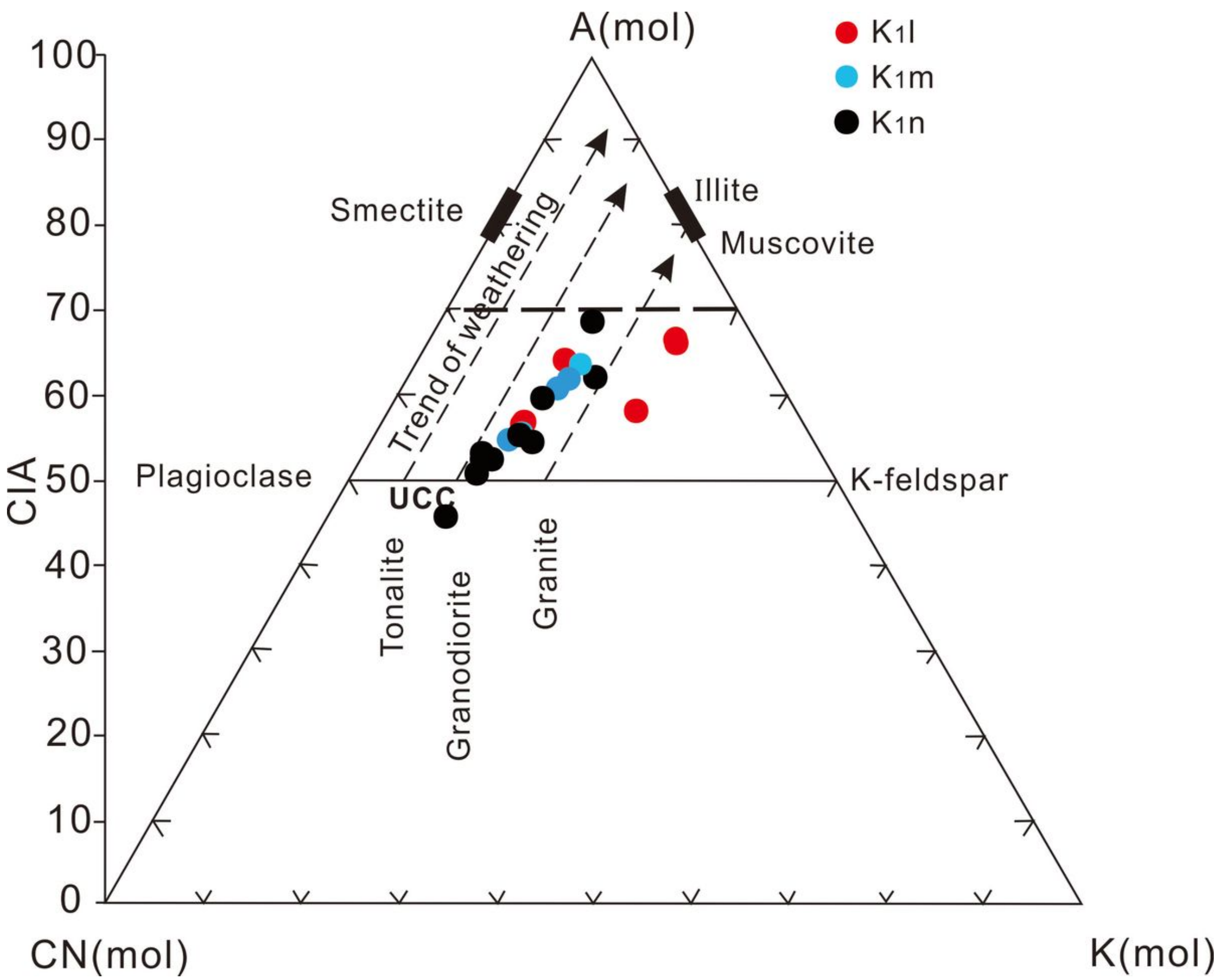

Figure 6

Al_2O_3-(CaO^* + Na_2O)-K_2O ternary diagram to infer the degree of weathering (in molar proportion).

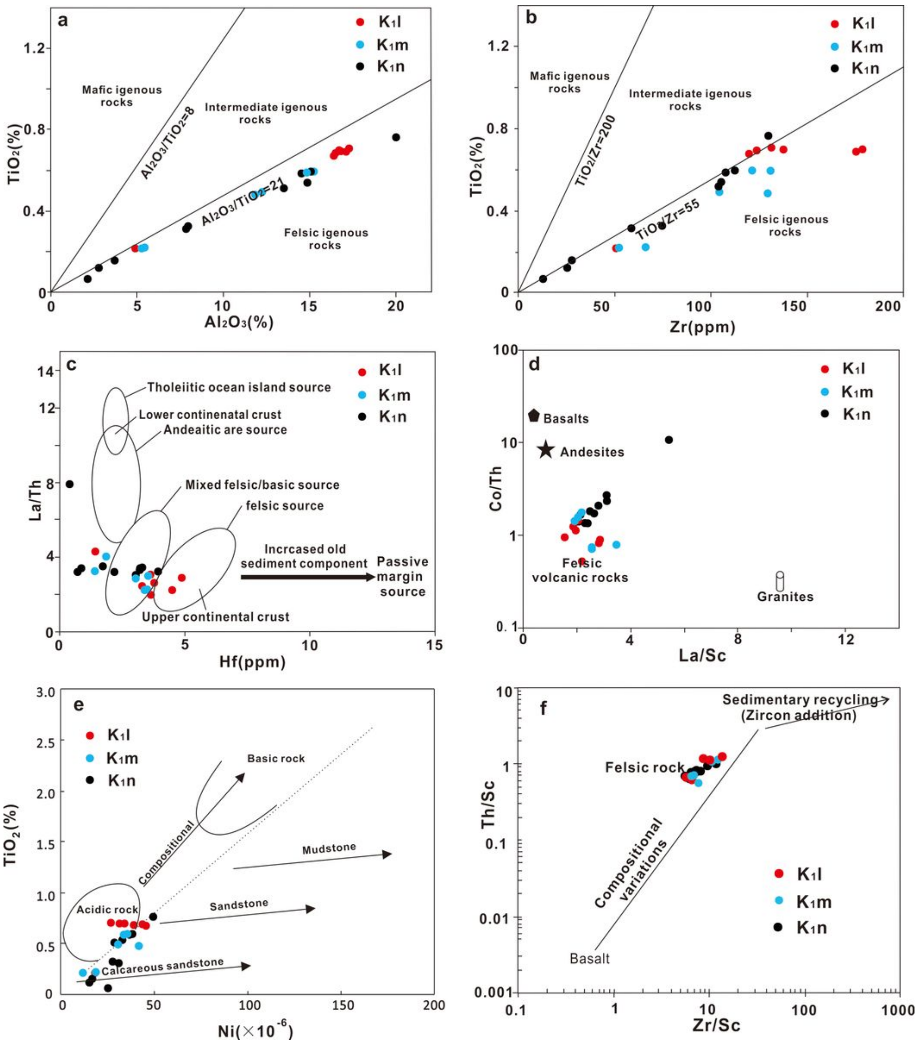

Figure 7

Bivariate plots for the Lower Cretaceous mudstones from the Liupanshan Basin. (a) TiO_2 vs. Al_2O_3; (b) TiO_2 vs. Zr; (c) La/Th–Hf; (d) Co/Th–La/Sc; (e) TiO_2 vs. Ni; and (f) Th/Sc vs. Zr/Sc.

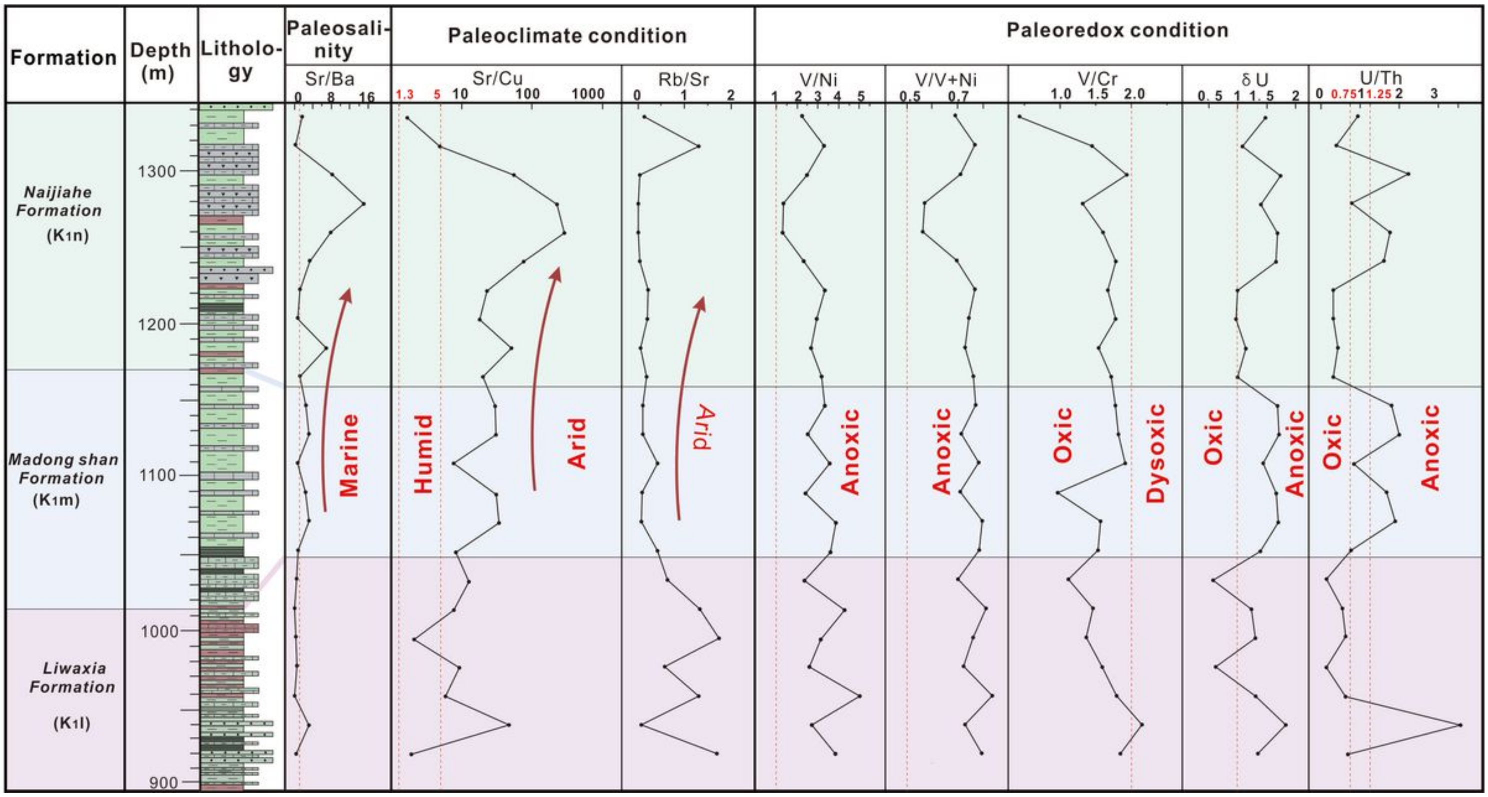

Figure 8

The indicators of paleosalinity, paleoredox, and paleoclimate conditions for the Lower Cretaceous mudstones from the Liupanshan Basin.

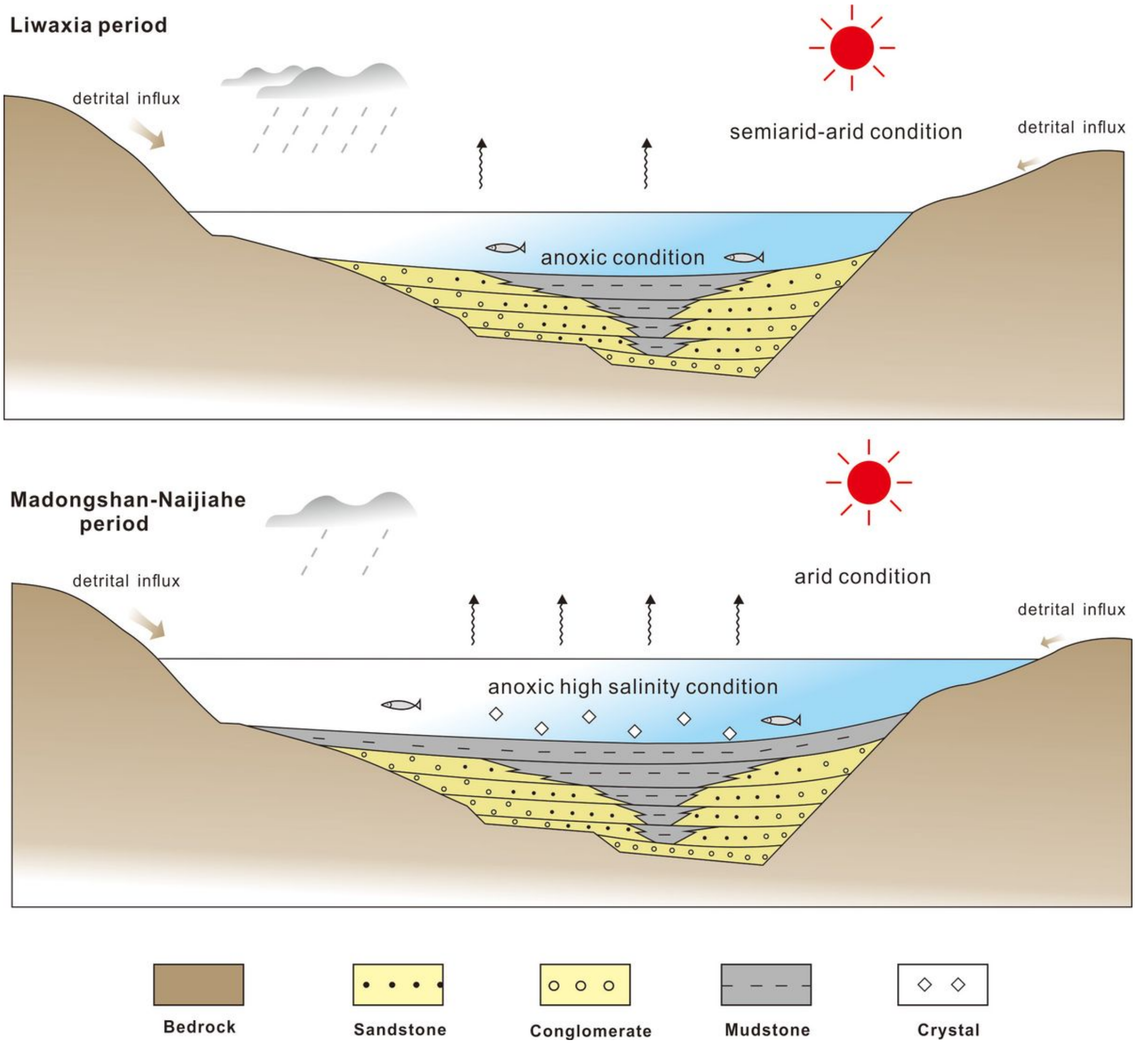

Figure 9

The sedimentary evolution model of the Liupanshan Basin during the Liwaxia-Naijiahe period.

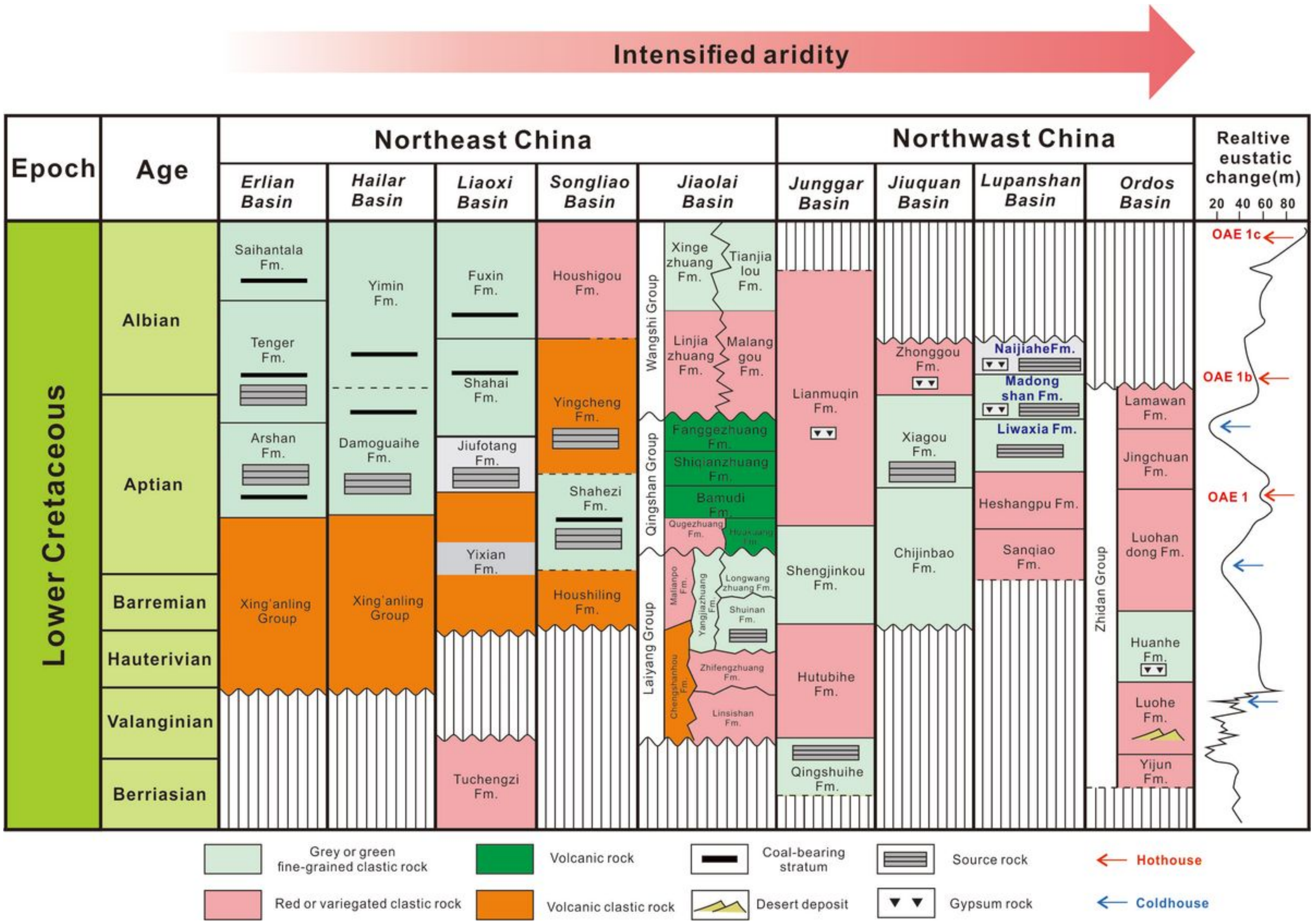

Figure 10

Relationship of sea level changes with early Cretaceous continental paleoclimate and sedimentary environment in northern China. Stratigraphic data of northern China from Cao (2018) and Xi et al. (2019), and relative eustatic change data after Sahagian et al. (1996).